UNIVERSIDADE FEDERAL DO RIO GRANDE DO SUL
INSTITUTO DE INFORMÁTICA
PROGRAMA DE PÓS-GRADUAÇÃO EM COMPUTAÇÃO

WESLEY FERREIRA DE FERREIRA

3D Human Body Processing and Automatic Measurements

Thesis presented in partial fulfillment of the requirements for the degree of Master of Computer Science

Advisor: Prof. PhD. Marcelo Walter

Porto Alegre
November 2023

CIP — CATALOGING-IN-PUBLICATION

de Ferreira, Wesley Ferreira

3D Human Body Processing and
Automatic Measurements / Wesley Ferreira de Ferreira. – Porto Alegre: PPGC da UFRGS, 2023.

55 f.: il.

Thesis (Master) – Universidade Federal do Rio Grande do Sul. Programa de Pós-Graduação em Computação, Porto Alegre, BR–RS, 2023. Advisor: Marcelo Walter.

1. Geometric Modeling. 2. Automatic Antropometrics Measurement. 3. Scanned Bodies. I. Walter, Marcelo. II. Título.

“Science, my lad, is made up of mistakes,
but they are mistakes which it is useful to make,
because they lead little by little to the truth.”

— Jules Gabriel Verne

ACKNOWLEDGMENTS

My acknowledgments, first, for my family, who never gave up on me, always comforting me in painful and stressful moments, especially my mom, who gave me millions of encouraging words and reminders not to overdo and take important rests. Secondly, I need to thank my old friends, with whom I don't lose contact, just chatting, chilling, and playing games randomly. The new ones, made during my master's degree, from graduate colleagues to undergraduate students, especially the *Meio Doidos* group, where I found friendship, comfort, kindness, and happiness even on the worst days. I'm thankful too to Roberto and Eliane, who act like father and mother to everyone who rents their housing, to my therapist Ediane Cappa, who kept me from freaking out during the COVID-19 pandemic and until I was comfortable in Porto Alegre, and to my Advisor, Prof. Marcelo Walter that guides me around the faced problems and gives me trust, understanding, and support during the master's degree time. I am thankful to my girlfriend, Flavia Santos, for her patience and support. Lastly, but not less importantly, I am thankful for Prof. Ph.D. Luciana Nedel who invited me last year to a research and innovation project that captivated me and allowed me to travel and meet new people.

ABSTRACT

Accurate and precise body measurements are crucial for several applications, such as calculating body composition, performing health evaluation, and clothes design. Studies sustain that advances in 3D scanning have become a faster alternative than traditional and sometimes manual strategies, despite discussions about precision and traditional anthropometric process compatibility. Our work presents an approach for automatically measuring 3D scanned bodies using curve-level slicing in a template-fitted and smoothed surface. We validate our approach by performing two experiments. In experiment one, our findings improve repeatability from previous state-of-the-art results by 14.2% and in experiment two by 16.6%. On compatibility, the first experiment improves state of the art by 32.2% and the second one by 18.6%. We also increment the number of measures that achieve strict error criteria defined by international standards in 14.3%. Furthermore, our technique provides other advancements in automatizing body measurements, e.g., standardized body representation and treatment of body scanning through a template fitting and a fully automatic measurement process.

Keywords: Geometric Modeling. Automatic Antropometrics Measurement. Scanned Bodies.

Processamento e medições automatizadas do corpo humano 3D

RESUMO

Medições corporais precisas e acuradas são cruciais para diversas aplicações, como composição corporal, avaliação de saúde e design de roupas. Estudos sustentam que os avanços na digitalização 3D se tornaram uma alternativa mais rápida do que as estratégias tradicionais e às vezes manuais, apesar das discussões sobre precisão e compatibilidade do processo antropométrico tradicional. Nosso trabalho apresenta uma abordagem para medir automaticamente corpos digitalizados em 3D usando corte em curvas de nivel em uma superfície suavizada e ajustada a um model. No experimento um, nossas descobertas melhoraram a repetibilidade dos resultados anteriores do estado da arte em 14,2% e no experimento dois em 16,6%. Em termos de compatibilidade, o primeiro experimento melhora o estado da arte em 32,2% e o segundo em 18,6%. Também aumentamos em 14,3% o número de medidas que atingem critérios de erro rigorosos definidos por padrões internacionais.. Além disso, nossa técnica fornece outros avanços na automatização de medidas corporais, por exemplo, representação corporal padronizada, tratamento das digitalizaçoes dos corpos através de um ajuste de modelo e um processo de medição totalmente automático.

Palavras-chave: Modelagem Geométrica. Medição Antropométrica Automática. Corpos Escaneados.

LIST OF ABBREVIATIONS AND ACRONYMS

2D	Two Dimensional
3D	Three Dimensional
ANOVA	Analysis of variance
ANSUR	The Anthropometric Survey of US Army Personnel
CAESAR	The Civilian American and European Surface Anthropometry Resource
HU	Head Unity
ICC	Intraclass Correlation Coefficient
ISO	International Organization for Standardization
MAD	Mean Absolute Deviation
PC	Principal Components
PCA	Principal Component Analysis
PSD	Pairwise Standard Deviation
SEM	Standard Error of Measurement
SMPL	A Skinned Multi-Person Linear Model

LIST OF SYMBOLS

ΔT	Variation of Number of Iterations
ΔPC	Variation of Principal Components
SS	Sum of Squares
df	Degrees of Freedom
MS	Mean Squares

LIST OF FIGURES

LIST OF TABLES

CONTENTS

1 INTRODUCTION

Many important applications demand accurate and precise measurements and measures[1] of the body: understanding body composition (PLEUSS et al., 2019; PADILLA; FERREYRO; ARNOLD, 2021), evaluating health risks (JEON et al., 2023), designing personalized clothes (ZAKARIA; GUPTA, 2019), creating ergonomic workstations (DIANAT; MOLENBROEK; CASTELLUCCI, 2018), and developing customized fitness programs (PEDRETTI et al., 2019). Researchers continue to explore new methods and technologies for improving the quality of measures nowadays. For example, 3D scanning technology has emerged as a *de facto* tool for body measurements, as it captures the shape and size of the body in a non-invasive and highly accurate way (RUMBO-RODRíGUEZ et al., 2021). Already in 2002, (ROBINETTE et al., 2002), the need for standards to provide sustainable development of comparable techniques became clear.

ISO 8559-1:2017 (ISO, 2017). Besides, **ISO 20685-1:2018** (ISO, 2018) and **ANSUR** *The Anthropometric Survey of US Army Personnel* (GORDON et al., 1989) are standards that define the minimum quality of measurements.

Despite the efforts to provide these standards, achieving the recommended level of quality in body measurements can be challenging, as it requires proper equipment, training, and experience. Even after meeting these requirements, measurement errors may still occur due to various factors such as movements during capture, loose clothing, posture, and body position (HU et al., 2021). Recently, Ballester et al. (2022) presented a large-scale comparison of various state-of-the-art measurement technologies as a statistical study of coherence between technologies and repetitions of the same technology.

1.1 Motivation

As discussed by Ballester et al. (2022), the systemic high variability and low agreement between experts and technologies make it harder to define ground truth for measurements and preferences for any particular measurement method. Therefore, consistent methods to quantify the quality of human body representation remain necessary. Our main motivation is to expand the comparative bases of 3D scanned body measurement techniques while increasing reliability and compatibility through our competitive ap-

[1] Along the text, we are treating the words measurement as the process and measure as the outcome of measurement.

proach, advancing the state-of-the-art by following the methodology presented by Ballester et al. (2022).

1.2 Goals

Using state-of-the-art industry standards, our main goal is to create a method that measures human bodies fast, automatically, and accurately following international standards. Specifically, we focused on computing anthropometrical measures extracted from digitized human bodies; an illustration of our expected input and output is presented in Figure 1.1. Our specific goals are:

- Create a systematic measurement process;
- Evaluate measures with state-of-the-art statistics;
- Compare measures with other state-of-the-art techniques.

Figure 1.1 – Illustration of expected input and output of our approach.

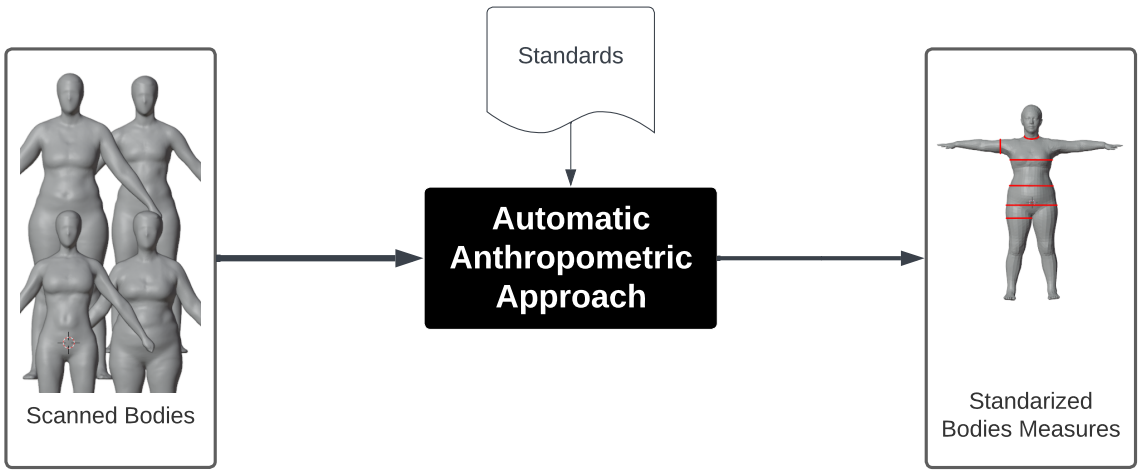

Source: The Author.

1.3 Work Structure

The rest of this work is organized as follows:

- **Chapter 2 - Theoretical Foundation:** Presents discussions of fundamental concepts for understanding this work;
- **Chapter 3 - Related Work:** Presents research correlated with this proposal;
- **Chapter 4 - Materials and Methods:** Presents the work's architecture, databases

used, and techniques applied to achieve the proposed goals;

- **Chapter 5 - Results and Discussions:** Presents the validation procedure, performed analysis, obtained results, and a discussion about results;
- **Chapter 6 - Conclusions:** Presents an overview of the presented work, faced challenges, and future work.

2 THEORETICAL FOUNDATION

This chapter introduces the main theoretical foundations for best understanding the presented work. The chapter starts with anthropometry concepts and applications, followed by concepts in Geometry Processing, and finishes with the statistics techniques used to validate the proposed method.

2.1 Anthropometry

Anthropometry is the science that studies human body measurements, particularly the measures of body size and shape. The term defines the complete collection, analysis, and communication process of the data (PHEASANT, 2002; ZAKARIA; GUPTA, 2019). As a science, anthropometry is useful in several application areas, as we can see next.

2.1.1 Anthropometry in Ergonomics

Anthropometry is an important area in ergonomics because it is a tool to design the environment according to human size and shape. The ergonomics term was coined in July 1949 by Hywell Murrell. Derived from Greek, it refers to the science of human beings and the working environment. Considering the work in a broader sense, ergonomics is concerned with the design of the tools for working (PHEASANT, 2002).

2.1.2 Anthropometry in Health Care

Anthropometric measures are a fundamental indicator for nutritional evaluation. With some limitations, it has good operation and accuracy. Body girths, diameters, and ratios are risk factors for cardiovascular and metabolic diseases (PADILLA; FERREYRO; ARNOLD, 2021; JEON et al., 2023). These metrics are also important tools for epidemiology study and clinical practice (SAMPAIO, 2012). Arm Girth, Bust Girth, Waist Girth, and Thigh Girth, used in this work, are some of the indicators of fat distribution and body composition. Figure 2.1 illustrates these girth measures.

Figure 2.1 – Health care important girths: Neck; Upper Arm; Bust; Waist; Hip and Thigh.

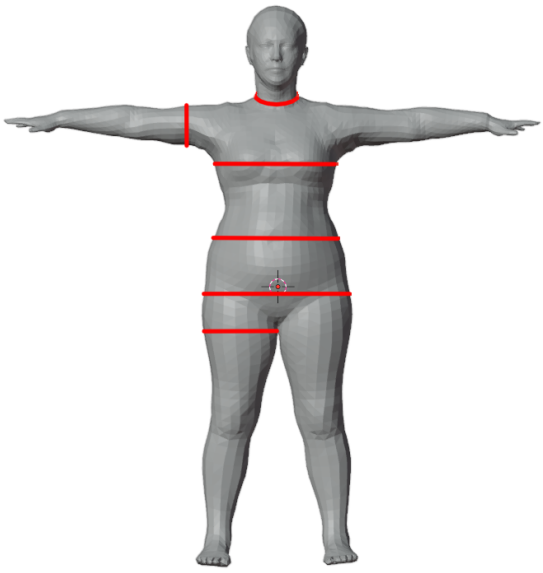

Source: The Author.

2.1.3 Anthropometry in Apparel Sizing

The apparel industry widely uses anthropometric techniques and measurement processes for garment design, converting customer measures to 3D models and assessing appearance and interaction with the body. With the advancements in digital anthropometry, the increment of anthropometric datasets is visible but still not largely internationalized (ZAKARIA; GUPTA, 2019). Figure 2.2 illustrates a garment fitting into a body.

Figure 2.2 – Illustration of "*garment*" fitting into a body.

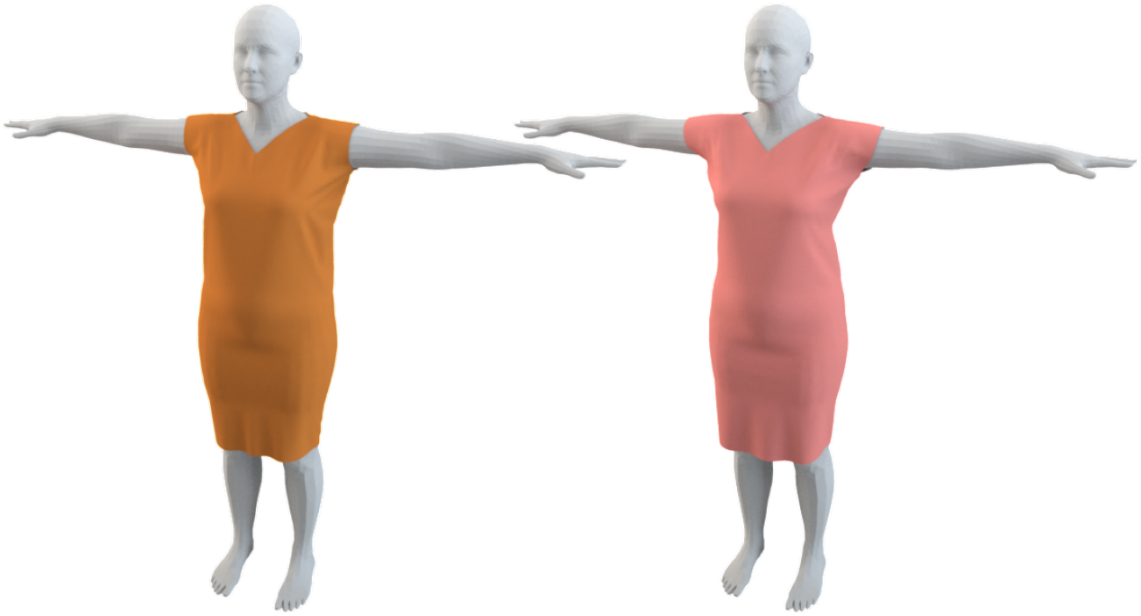

Source: Korosteleva and Lee (2022).

2.2 Geometry Processing

Geometry Processing is a Computer Graphics area that studies the manipulation of digital shapes, usually presented as triangle meshes, through processing algorithms (YANG et al., 2021).

2.2.1 Surface Registration

Scanning processes of real objects only capture partial surfaces, and the major task in getting a complete 3D model is to combine partial scans into one. The surface registration process consists of putting these partial scans in corresponding positions in space, minimizing the distance between correspondences, and merging them (BÆRENTZEN et al., 2012). In our case, the surface registration will be useful to match a template body to an original raw model, and this process was made using the SMPL template (LOPER et al., 2015), presented later.

Figure 2.3 – SMPL template registration of raw high poly model sample: Raw model at the front, SMPL model at the back.

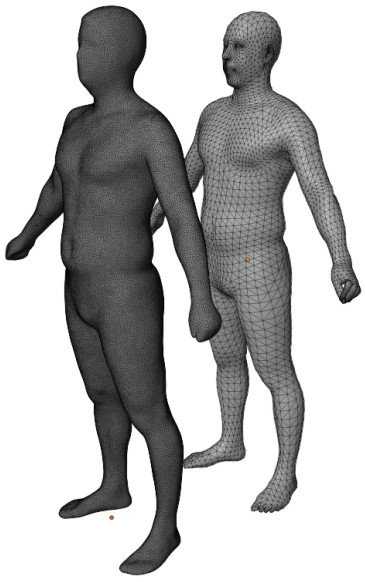

Source: The Author.

2.2.2 Subdivision Surfaces

The subdivision surface operation can be viewed as a refining operation over a graph representing a geometry through local operations. Usually used by graphics designers to refine and cut off sharp edges in polyhedral objects, the meshes, when recursively applied, converge to smoothest representations (PETERS; REIF, 2008).

In Computer Graphics, the dominant mesh object representation varies according to context. In modeling, for example, the dominant techniques were splines and quad-based representation, while in rendering, the dominant representation was the triangle (HUGHES; FOLEY, 2014). Therefore, different subdivision surface techniques must be applied for different situations.

The most common technique applied to quad-based representation was the Catmull-Clark (CATMULL; CLARK, 1998) while the Loop Subdivision (LOOP, 1987) is more suitable for triangle-based representations (ZHOU; BOONSTRA; KOSINKA, 2023). Figure 2.6 presents a sample of body model subdivision.

Figure 2.4 – Catmull-Clark subdivision surface technique illustration.

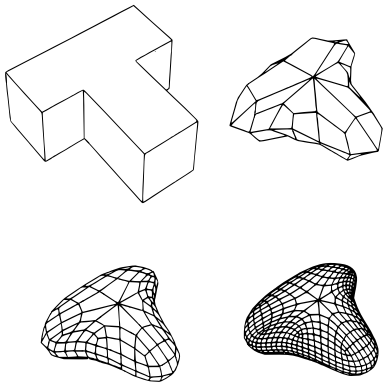

Source: Loop (1987). Modified by the author.

Figure 2.5 – Loop subdivision surface technique illustration.

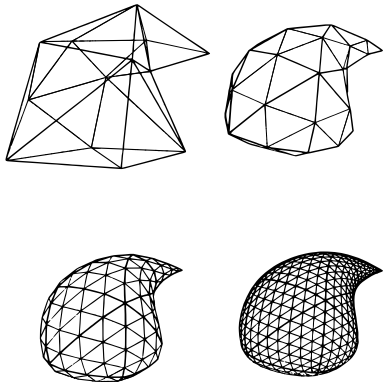

Source: Loop (1987). Modified by the author.

Figure 2.6 – Subdivision surface example: Lower polygon count at left (a), higher polygon count at right (b).

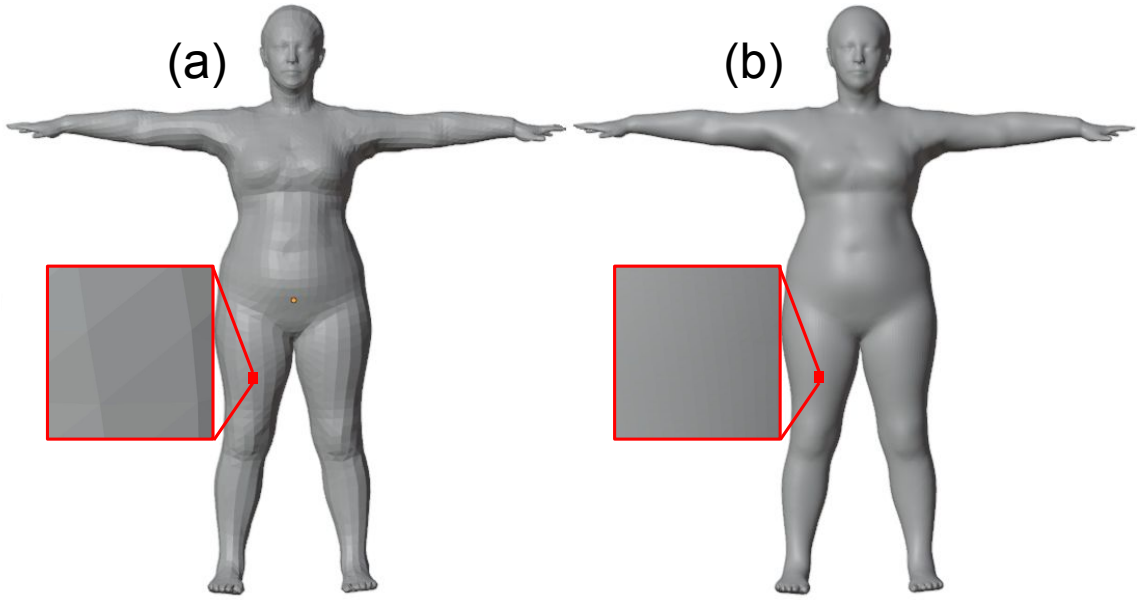

Source: The Author.

2.2.3 Level Curves

Level Curves, also called *Contour Lines*, are an important tool to represent functions of two or three variables in a plane, most typically used in topography to represent height maps. It is also an important technique for analyzing a function's behavior according to the variation of one variable. Level curves are usually obtained by slicing the interest function with horizontal planes (HUGHES-HALLETT; GLEASON; MCCALLUM, 2012). Figure 2.7 illustrates a level curve in a land relief mapping.

Figure 2.7 – Illustration of land relief mapping by contour lines.

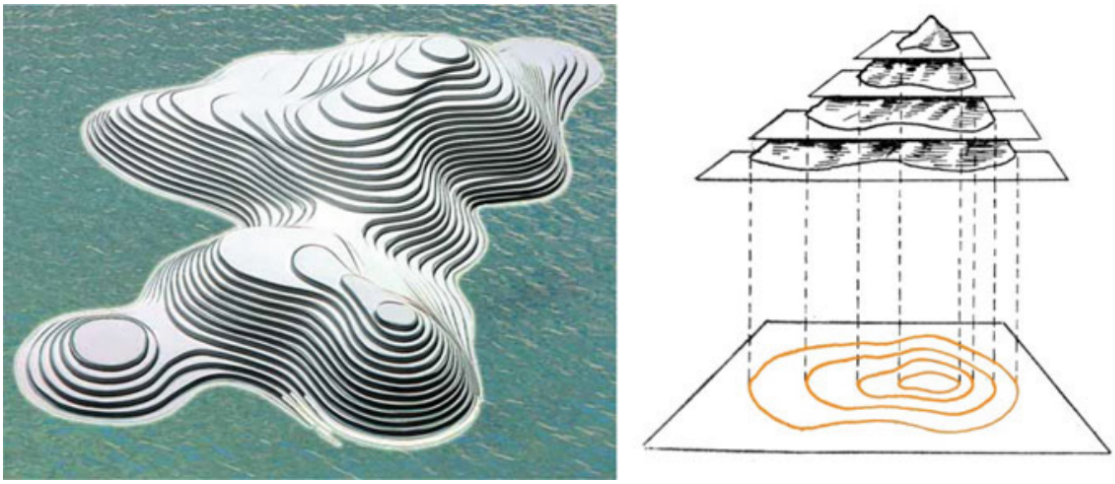

Source: Markoski and Markoski (2018).

Figure 2.8 – Visual interpretation of barycentric coordinates.

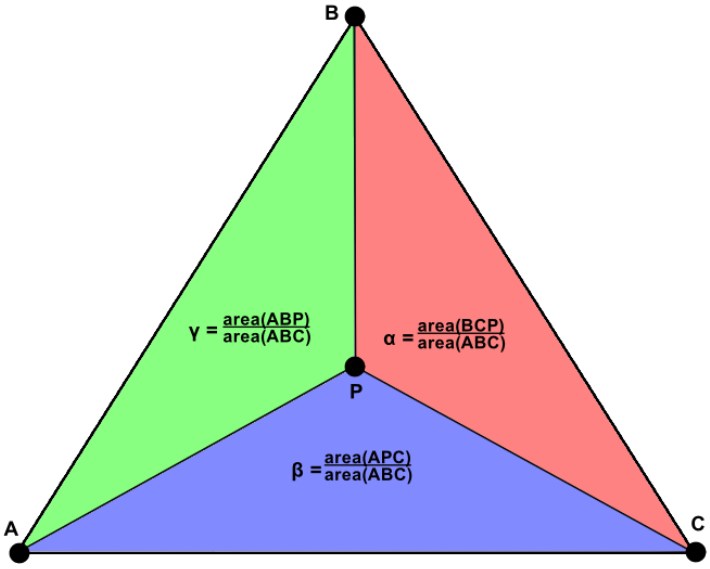

Source: The Author.

2.2.4 Barycentric Coordinates

Triangles are an important concept in geometry. They consist of three vertices A, B, C, and the edges connecting them. Each point P inside a triangle can be represented as a weighted average of the vertices' coordinates using barycentric coordinates α, β, γ such that $P = \alpha A + \beta B + \gamma C$ (HUGHES; FOLEY, 2014). Figure 2.8 gives a visual interpretation of barycentric coordinates according to the three triangle vertices.

2.3 Statistics

According to Devore (2015), "The discipline of statistics provides methods for organizing and summarizing data and drawing conclusions based on information contained in the data."

The statistical methods presented in this section were provided by Ballester et al. (2022) and focused on evaluating anthropometric techniques. This section is divided into Repeatability and Compatibility Analysis.

2.3.1 Repeatability Analysis

In the repeatability analysis, we are interested in evaluating the degree of agreement between the two repeated measurements made from the same method on the same subject. We present below the MAD and SEM indexes. The closer the results are, the more internal consistency the method has.

2.3.1.1 Mean Absolute Deviation

The mean absolute deviation (MAD) measures the variability of the data, which is calculated by taking the absolute value of the difference between each data point and the data set's mean and then finding the average of those absolute differences. Equation 2.1 shows the formula to calculate the mean absolute deviation.

$$MAD = \frac{\sum_{i=1}^{n} |x_i - \bar{x}|}{n} \tag{2.1}$$

2.3.1.2 Analysis of variance (ANOVA)

According to Devore et al. (2012), "The analysis of variance, or more briefly ANOVA, refers broadly to a collection of statistical procedures for the analysis of quantitative responses." Being capable of leading various types of experiments, with one or two factors analyzed fixed or randomly, is probably the most useful technique in statistical inference. Table 2.1 present the ANOVA equations according to Weir and Vincent (2020). $\bar{X}_{group}$ represents the average between all values in the same experiment while $\bar{X}_{grand}$ represents the average between all the values in all experiments, k represents the number of subjects while N represents the total number of samples.

Table 2.1 – One-Way ANOVA equations table.

	SS	df	MS	F
Between	$\Sigma(\bar{X}_{group} - \bar{X}_{grand})^2$	$k-1$	$\frac{SS_B}{df_B}$	MS_B/MS_W
Within	$\Sigma(X - \bar{X}_{group})^2$	$N-k$	$\frac{SS_W}{df_W}$	
Total	$\Sigma(X - \bar{X}_{grand})^2$	$N-1$		

2.3.1.3 Intraclass Correlation Coeficcient

The intraclass correlation coefficient (ICC) is a statistical measure that compares the variance within and between clusters, i.e., it formally quantifies reliability when the

same variable is measured on multiple occasions (WEIR; VINCENT, 2020). Calculated through the ANOVA variance components, it ranges from 0 to 1, with higher values indicating greater reliability or consistency between measurements. A value close to 0 indicates a low agreement between measurements, while a value close to 1 indicates a strong agreement. Various methods of calculating ICC were presented by Weir and Vincent (2020), e.g., the related to one-factor ANOVA with fixed factors, used in this work, presented in Equation 2.2. The ICC values close to 1 mean low variability within subjects.

$$ICC = \frac{MS_B - MS_W}{MS_B + df_B MS_W} \tag{2.2}$$

2.3.1.4 Standard Error of Measurements

The standard error of measurement (SEM) is an absolute estimator of the reliability of a test, meaning it has the units of the test being evaluated and is not sensitive to the *between-subjects* variability of the data. Furthermore, SEM is an index of the test's precision or trial-to-trial noise and reflects the consistency of scores within individual subjects (WEIR; VINCENT, 2020). The SEM score reflects the variability within measurements on the same subject. We expect low scores when the measurements are close, i.e., the test has strong internal consistency or reliability. SEM is mainly independent of the population from which the results are calculated. It is argued to reflect an inherent characteristic of the test, irrespective of the subjects from which the data is derived (WEIR; VINCENT, 2020). Equation 2.3 presents how to calculate the standard measurement error, and it is clear that SEM and ICC values vary oppositely.

$$SEM = \sigma\sqrt{1 - ICC} \tag{2.3}$$

2.3.2 Compatibility Analysis

In the compatibility analysis, we want to evaluate the agreement's degree between the measurements from the two methods on the same subject. We present the PSD metric next.

2.3.2.1 Pairwise Standard Deviation

The pairwise standard deviation (PSD), also referred to as the standard deviation of the differences between pairs, is a statistical metric commonly used to measure the variability or dispersion of differences between two or more evaluators of the same subject measure (BALLESTER et al., 2022). This metric provides information on the level of agreement or disagreement between evaluators and the distribution of their scores. In other words, PSD indicates how much variability exists among evaluators' scores when assessing the same subject (BALLESTER et al., 2022).

When using SEM, we calculate the consistency of each evaluator and the differences between each pair of evaluators' scores. The standard deviation of the differences plus the mean of consistencies are determined. Equation 2.4 presents how the pairwise standard deviation was calculated where j and l represents the compared techniques.

$$PSD_{jl} = \sqrt{\sigma^2_{y_j - y_l} + \frac{SEM_j^2}{m} + \frac{SEM_l^2}{m}} \tag{2.4}$$

3 RELATED WORK

This chapter presents the most relevant works related to the proposed approach. This section was divided into Related Work Mapping, Anthropometric Databases, 2D Measuring Approaches, 3D Measuring Approaches, Human Body Representation, and Anthropometric Measures Validation.

For relevant papers, we searched the IEEE Xplore, ACM Digital Library, and Science Direct bibliographic databases. To complement the discussion, we selected the most relevant and recent work found, presented by Nourbakhsh Kaashki, Hu and Munteanu (2021), and applied a snowballing process, that is, scanning the references and the references of the references through missing relevant papers. In addition, we included already-known relevant works and guidelines. The relevant works discussion for our context will be described next.

3.1 Anthropometric Databases

Gordon et al. (1989) was probably the first anthropometric database with general guidelines to proceed with anthropometric surveys. In their work, nearly 4,000 military personnel were measured, with more than 140 measures taken by experts.

In 2002, the CAESAR dataset (ROBINETTE et al., 2002) provided more than 4400 subjects scanned in three poses, illustrated in Figure 3.1, along with demographic information and anthropometric data, following international standards. In a collaborative effort of three countries, the United States, the Netherlands, and Italy, and with the support of several industries, it was developed over three years. Being probably the first large anthropometric dataset with 3D body scans, the availability of this base has significantly advanced research in the 3D anthropometry area.

More than a decade later, Gordon et al. (2014) conducted an anthropometrical study including around 90 measures within the United States of America National Army with 6,000 subjects. They presented measurement results comparing four different measures and a whole-body scanner.

Yan, Wirta and Kämäräinen (2021) generate a Finish anthropometric database with 3D scanned bodies. Unfortunately, due to legal restrictions, they just provided fitted SMPL models. They also provided a 2D anthropometric measurement approach that will be discussed next.

Figure 3.1 – Sample of three digitized poses taken by the CAESAR study of a subject.

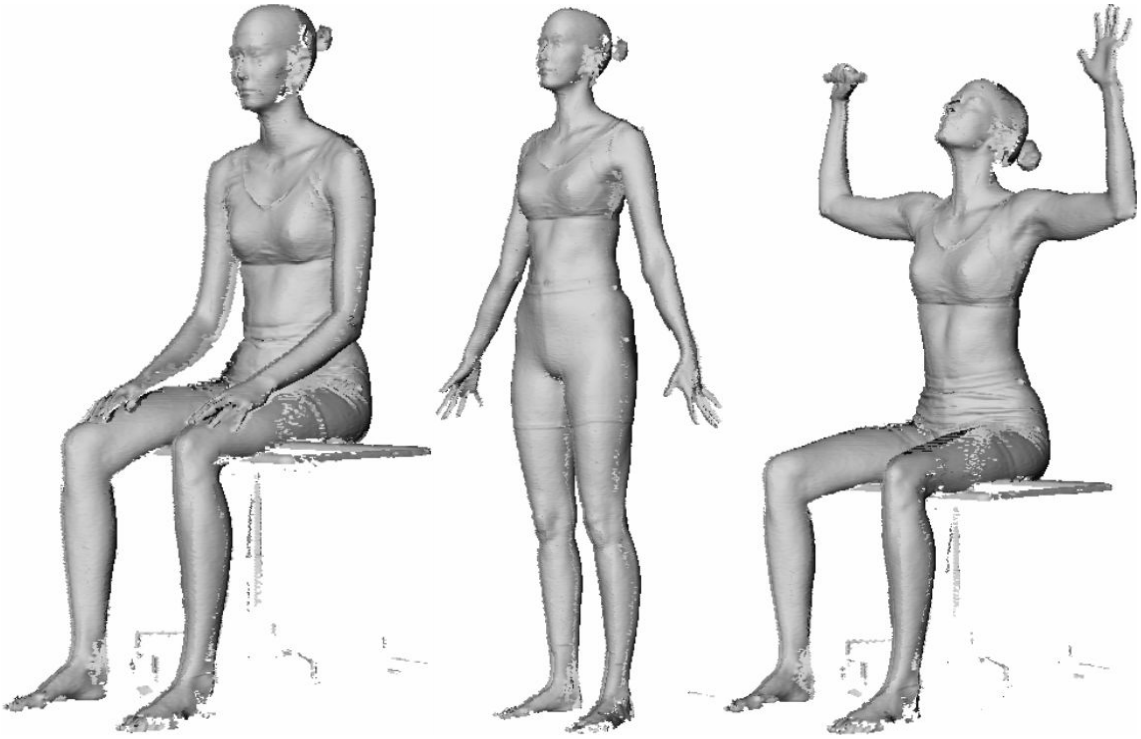

Source: Robinette et al. (2002). Modified and grouped by the author.

3.2 2D Measuring Approaches

Various approaches employ human body silhouettes, referred to here as 2D approaches, in combination with RGB and RGB-Depth data. These methods also incorporate advancements in laser scanner technologies for analyzing the body surface during digital anthropometry. These works used both traditional computer vision approaches (KOHLSCHÜTTER; HEROUT, 2012; BALLESTER et al., 2016; LIN; WANG, 2011; BENABDELKADER; DAVIS, 2006; DAO; DENG; CAI, 2014) as well as machine learning techniques (NGUYEN et al., 2016; De Souza et al., 2020; KRZESZOWSKI et al., 2023). No large discussions were provided here because of our focus on 3D approaches.

3.3 3D Measuring Approaches

Jones and Rioux (1997) introduced the automatic measurement of human bodies. They presented the first insights into the resolution parameters of automatic measurement applications. They also discuss the cost of traditional versus automated measurements, concluding that automated systems are more cost-effective, producing larger and more precise datasets. Paquette et al. (2000) evaluates the results produced by comparing two

body scanners with traditional techniques. Their study demonstrates that the two scanners yield contrasting results compared to traditional techniques: one producing lower values and the other higher values. However, they conclude that it is currently feasible to develop these techniques further.

Leong, Fang and Tsai (2007) described the evolution of 3D anthropometry techniques and scanners as well as described a method for identifying anatomical landmarks and anthropometrical features through depth maps derived from 3D models; an illustration of the process is presented in Figure 3.2. They claim their results are compatible with ANSUR (GORDON et al., 1989) MAD thresholds in evaluated measures. Unfortunately, their study deals with the upper body, not considering the lower body and arms. Lovato et al. (2009) described a method for pose estimation and body segmentation to detect feature points to assist semi-automatic measurements through geodesic distances. They assume a small subject set and non-negligible differences from manual measurements without comparing their results with any threshold.

Figure 3.2 – Illustration of the measure extraction process by Leong, Fang and Tsai (2007): (a) point cloud; (b) depth map; (c) measures from depth map.

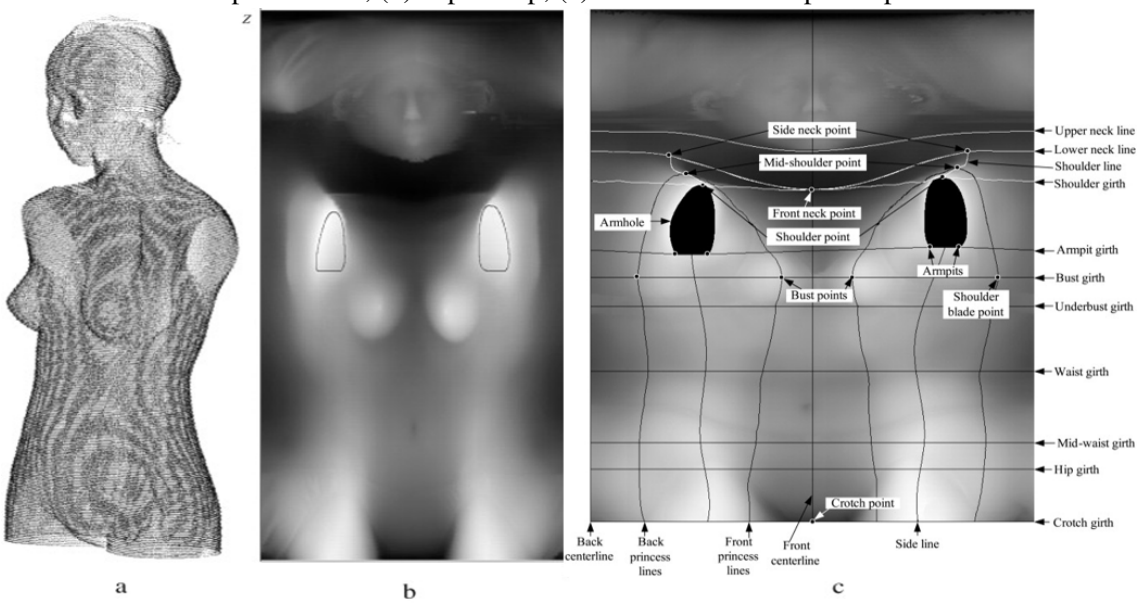

Source: Leong, Fang and Tsai (2007). Modified and grouped by the author.

In their pioneering work, Tsoli, Loper and Black (2014) introduced a template registration approach to represent human bodies. They utilized the SCAPE template (ANGUELOV et al., 2005) and triangle deformations to estimate linear distances. Furthermore, they employed a combination of triangle deformation and edge lengths to calculate a low-dimensional representation. This was achieved through Principal Component Analysis (PCA) and Elastic Net regression (ZOU; HASTIE, 2005) for predicting

measurements. Even using the large CAESAR (ROBINETTE et al., 2002) dataset for training, they present errors above ANSUR thresholds, claiming even so that the results are sufficient for real applications.

Markiewicz et al. (2017) is the first work to consistently frame their results and measurement errors according to ISO 20685-1. They proposed a measurement approach based on body segmentation and anatomical point search in volumes of interest in the body surface, using maximum and minimum values of Gaussian curvature to segment regions. They also discuss whether traditional manual measurement approaches should be treated as the ground truth, even if these measures were the best comparison data at the time. Xiaohui et al. (2018) proposed an approach to calculate human body size by extracting focal features of the body through a random forest regression analysis of geodesic distances between interest points calculated through a heat kernel. The authors claim their method leads to robust and accurate feature extraction and size measurement for 3D human bodies in distinct postures and shapes with holes and noise.

Nourbakhsh Kaashki, Hu and Munteanu (2021) presented a recent technique to measure the human body by cutting planes in the SMPL template-fitted artificially created models. They manually select the cutting planes in their base model in the template according to ISO 8559-1 (ISO, 2017). The body measurements use a neural network prediction, like the template-fitting process. Figure 3.3 illustrates the process adopted by the authors.

Figure 3.3 – Illustration of the measurement process by Nourbakhsh Kaashki, Hu and Munteanu (2021).

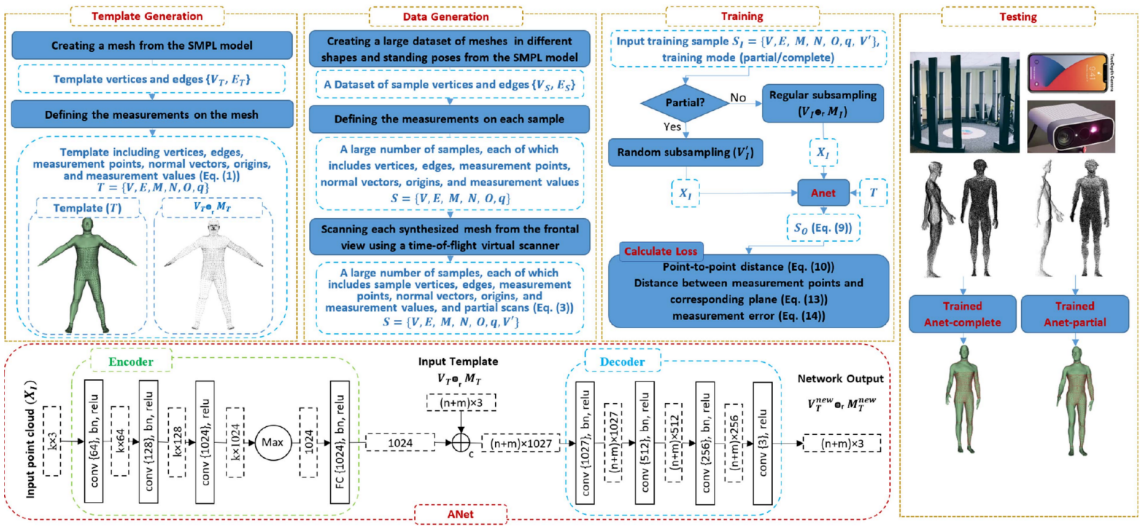

Source: Nourbakhsh Kaashki, Hu and Munteanu (2021).

3.4 Human Body Representation

Here, we present the main approaches for digitally representing human bodies in 3D shape and pose meshes, allowing better control and manipulation.

- SCAPE (Shape Completion and Animation of People) (ANGUELOV et al., 2005), is a data-driven method for the deformation and animation of human body shapes. Their solution builds a skeleton from a single scan and a motion capture sequence of the same person. From this skeleton, a pose-deformation model is learned that allows animation.
- The SPRING (Semantic Parametric Reshaping) (YANG et al., 2014) work presented a way to parametrize human bodies semantically. They split the process into two parts: *Global* and *Local* mappings. The global mapping is similar to previous works and is responsible for the overall shape and pose transformations. The local mapping uses linear regression to define if some semantic parameters impact shape deformation based on geodesic distances and certain thresholds, thus avoiding undesired side effects on different body parts.
- The *SMPL - A Skinned Multi-Person Linear Model* (LOPER et al., 2015) is a vertex-based linear model that presents a standardized and easy-to-use representation of human shape and pose, trained from thousands of scanned bodies in different poses. Each SMPL human model is represented by a triplet (β, θ, τ), where β represents the body shape in the form of Principal Components (PC), θ represents the body pose, and τ represents the body's position. Figure 3.4 presents a sample of the shape and pose modeling according to the SMPL model.

Figure 3.4 – SMPL model. (a) Template mesh blend weights; (b) Identity-driven blend shape contribution; (c) Pose blend shapes contribution; (d) Deformed vertices for the split pose.

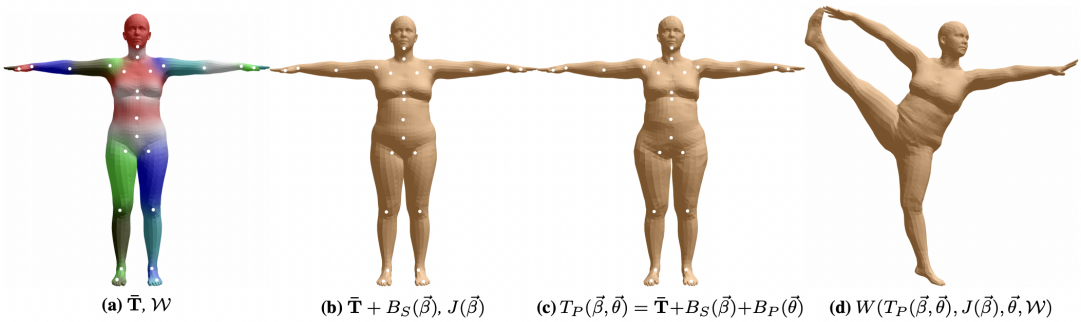

Source: Loper et al. (2015).

- The BOSS: Bones, organs and skin shape model (SHETTY et al., 2023) very re-

cently expanded the SMPL model (LOPER et al., 2015) with an internal representation of the human body, adding bones and organs through an optimization process and maintaining the SMPL principal components based representation.

3.5 Anthropometric Measures Validation

In 2010, Han, Nam and Choi (2010) evaluated the quality of measures from the Size Korea study. At that moment, the state-of-the-art techniques proved incapable of achieving the ISO 20685 (ISO, 2018) restricted thresholds.

Considering the increasing number of automatic human body measurement competitor techniques and the lack of clear comparison metrics, Ballester et al. (2022) presented a study assessing how measurement techniques compare. They defined 13 measurement *stations*: five measurement experts, four specialized 3D scanners, and four smartphone applications. One of their main results was that the discussed measurement techniques exhibit high repeatability but low compatibility. The study arrived at this conclusion by evaluating eleven measures taken twice by each station and statistically comparing the consistency of measurements within and between stations.

The ISO compatibility methods proved not practical for this type of assessment because of the high repeatability but low compatibility between stations. Despite the presence of measurement experts, the low compatibility between stations highlights the need for alternative methods for real-world scenarios. Then, references benchmarks and calculated values in the study could help to establish new criteria (BALLESTER et al., 2022).

3.6 Discussion

In the following section, we propose applying the newest and complete international standard of anthropometric measurements, ISO 8559-1 (ISO, 2017), to a smoothed SMPL template of real human bodies. We use an optimization process to create an automatic digital measurement process with quality bounds defined by ISO 20685-1 (ISO, 2018). Our validation uses the statistics proposed by Ballester et al. (2022) for compatibility with the ISO and the other methods. Apart from the other methods, we focus together on an automatic, deterministic, and standardized representation and measurement process.

4 MATERIALS AND METHODS

This chapter overviews our database and the approach developed to achieve the proposed goals. The chapter was divided into a section describing in detail the used dataset and the three-step approach: *i) body preprocessing*, where we convert a set of 3D body meshes we want to measure into an equivalent SMPL template; *ii) curve selection*, where we first compute an average body as the base body from our body set, and on this base body, we find the best corresponding curve on the body's surface for each desired measure; and *iii) curve application*, where we transfer the curves from the base body to all other bodies in the set, finalizing the measurements. Figure 4.1 presents an overview illustration of our approach.

Figure 4.1 – Overview of our technique. Given our respectively divided curve selection and curve application validation sets, we perform a sequence of steps for each set according to the pipeline. For each step, we provide more details in the corresponding section.

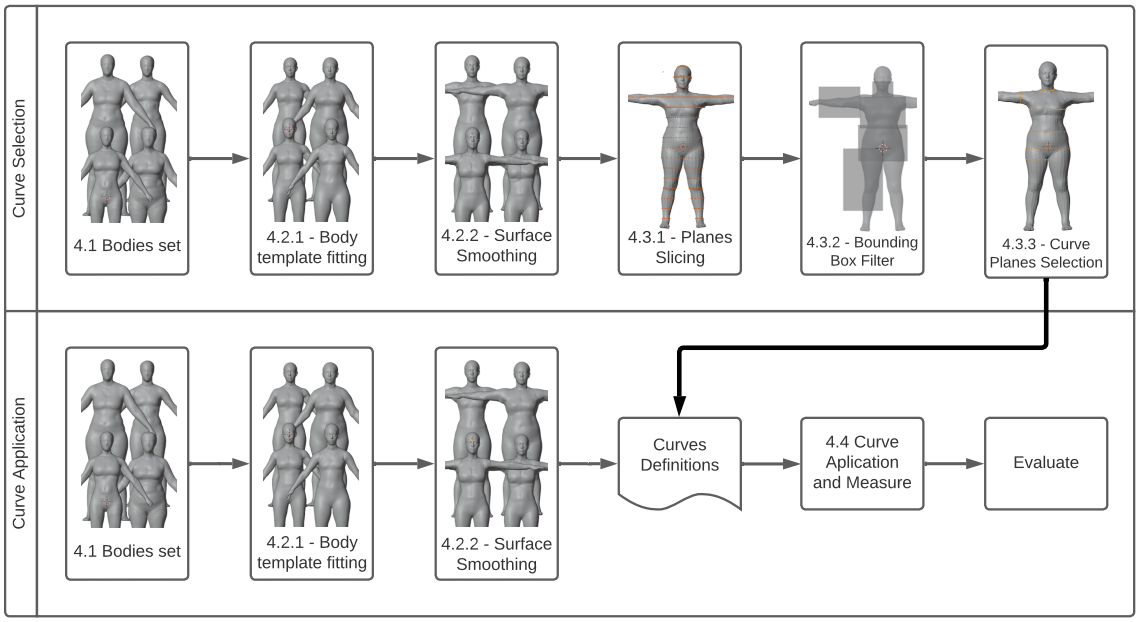

Source: The Author.

The experiments were executed in an Intel Core I7 9700K with an Nvidia Quadro P6000 and 32GB RAM machine, and the execution time, as well as the number of required executions of each step of our approach, is presented in Table 4.1.

Table 4.1 – Time (in seconds) to perform each step of the approach and number of execution times of each one.

	Time (s)	Nº of times
4.2.1 - Template Fit	113	Per Body
4.2.2 - Surface Smoothing	3	Per Body
4.3.1 - Plane Slicing	471	One Time
4.3.3 - Curve Selection	617	One Time
4.4 - Curve Application	10	Per Body

4.1 Bodies Datasets

To develop the proposed approach, we used the bodies and measures provided by Ballester et al. (2022) database due to their public availability, the size of the dataset, and the availability of different possibilities of reference measures. This dataset was divided into two subsets, phase 1 and phase 2. Each station measured a different subset of subjects, with two repetitions for each subject. We defined two datasets: *a)* MOVE4D and Expert 1, and *b)* SS20 and Expert 1. MOVE4D and SS20 are the best quality 3D scanners from Phase 1 and Phase 2, respectively. The selected Expert is the most proficient measurer. The size of each experiment phase was presented in Table 4.2.

Table 4.2 – Number of subjects of each scanner divided by gender, phase number, and number of repetitions.

	Phase	Male	Female	Repetitions
MOVE4D	1	36	36	2
SS20	2	20	39	2
Expert	1 and 2	56	75	2

In the template fitting and surface smoothing, all the bodies from MOVE4D and SS20 were submitted, including repetitions. In the curve selection, a subset to generate reference curves, the first repetition of subjects from MOVE4D, was selected. All MOVE4D bodies, including repetitions, were selected to compose the curve application and validation. The entire SS20 dataset was used in the curve application without interfering with the selection.

4.2 Body Preprocessing

Body preprocessing was divided into two steps. We first perform the SMPL template fitting and then apply surface smoothing. These steps will be explained in detail next.

4.2.1 Template Fitting

In this step, we perform template fitting on the meshes representing the human bodies. Having all the bodies in the same template allows us to design a uniform data treatment. In our case, we convert the original geometry into an equivalent SMPL template mesh for each body. In the SMPL template, the complexity of the body shape is expressed through Principal Components that represent the body in a small dimension set of parameters. Computationally, we designed a procedure that, for each body, iteratively finds an appropriate number of PCs to represent the body shape as SMPL within some error criterion.

Our comparison between the original body and the template-fitted uses the *point cloud to mesh distance* from the Open3D Library (ZHOU; PARK; KOLTUN, 2018). It calculates the distance between each vertex in the source – the original mesh – and the closest face in the target mesh, resulting in a mean squared distance. The Equation 4.1 presents the error minimization goal: N_i represents the number of vertices in the original mesh while N_j represents the number of faces in the template mesh; f represents the distance between each point p_i in the original mesh and the closest triangle t_i in the template, while g represents the distance between each triangle t_j in the original mesh and the closest point p_j in the template.

$$\epsilon = \frac{1}{N_i}\sum_{i=0}^{N_i} f(p_i, t_i)^2 + \frac{1}{N_j}\sum_{i=0}^{N_j} g(t_j, p_j)^2 \tag{4.1}$$

Given the complexity and the non-deterministic nature of the adopted template fitting process, we realized a set of experiments aiming to discover the best cost-benefit combination size and increments of SMPL PCs (β parameters). The first experiment developed was searching for an optimal number of SMPL PCs to represent a given shape using the Adam optimizer (KINGMA; BA, 2014) with a learning rate of 0.2. This rate is the standard learning rate proposed by the original SMPL authors on their legacy fitting process, with worst-case loss stop criteria of the average error of $0.02mm$ and processing time stop criteria of 10000 iterations. We opted for these two stop criteria due to the exponential error decay in the fitting process. We repeat the procedure ten times for each body to improve reliability in the result since the Adam optimizer has random initialized internal parameters.

The results of this experiment about the number of components that compose the

template fitting are presented in Figure 4.2. The results regarding the optimization iterations are presented in Figure 4.3.

Figure 4.2 – Logarithmic error decay between the original mesh and the template fitting according to the number of SMPL principal components.

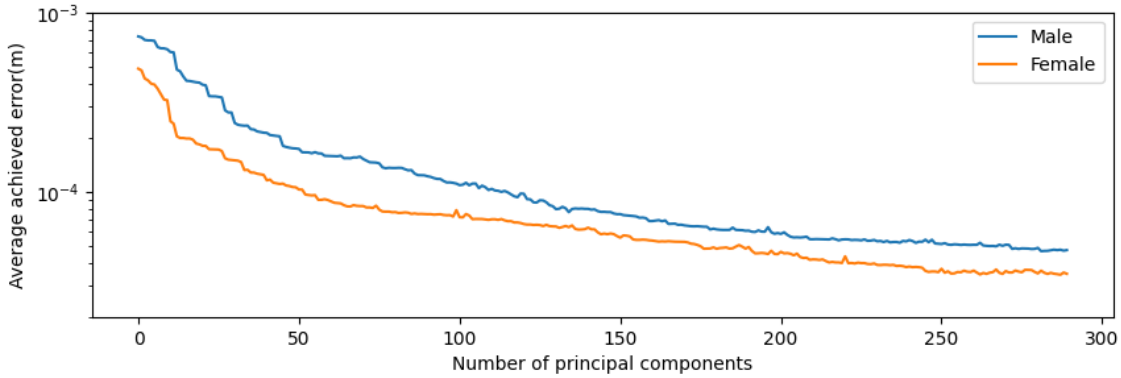

Source: The Author.

Figure 4.3 – Logarithmic error decay between original mesh and the template fitting according to the number of interactions of Adam optimization process.

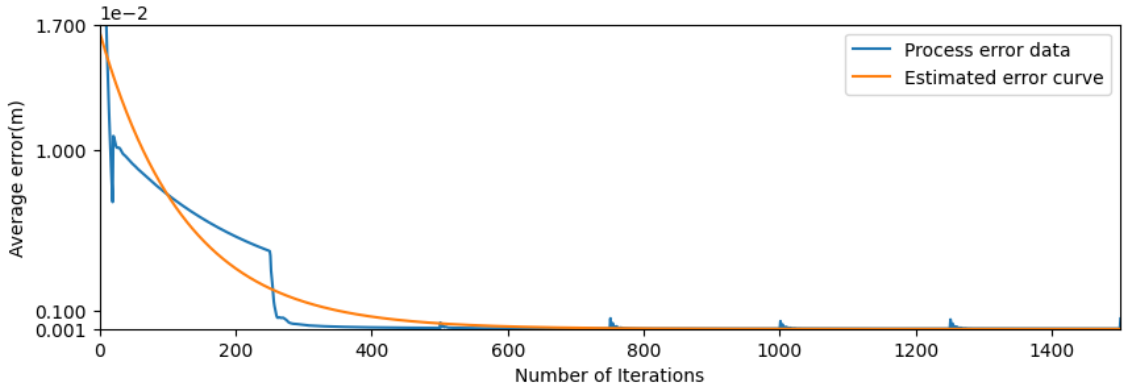

Source: The Author.

By gradually incrementing the number of principal components, we guarantee that the most relevant components in the representation space are optimized first, taking less time with minor differences in the final part of optimization. This process generates a combination of increment sizes for the principal components (ΔPC) and the time between increments (ΔT). We then search for the best processing time by searching the $(\Delta PC, \Delta T)$ parameter space, described in Table 4.3.

The ΔT values less than 50 give Adam no time to improve the error, whereas increment intervals greater than 500 take more than 10 minutes to achieve the goal error. On the other hand, values of ΔPC less than 50 represent a small number of increments resulting in a large number of intervals to achieve the maximum number of components. Lastly, increment sizes greater than 250 take too long to achieve the total capacity of the

Table 4.3 – Description of the $(\Delta PC, \Delta T)$ parameters search space for best cost-efficient template fitting optimization process.

	min	**max**	**increment**
ΔT **(iterations of Adam)**	50	500	50
ΔPC **(increment sizes)**	50	250	10

principal components. Given that, we search the values of $(\Delta PC, \Delta T)$ in the parameter spaces that minimize the template fitting execution time to achieve the $0.2mm$ error according to the point mesh distance described before.

This experiment detects the best configuration of ΔT around 250 according to Figures 4.4 and 4.5. With this defined value, we evaluate ΔPC according to the processing time to obtain the best combination of these two factors. As illustrated in Figures 4.6, 4.7, and 4.8, we found the best result in the combination $(250, 100)$. The final configuration brings fewer than a thousand interactions to achieve the error bound. Figure 4.9 (a,b) shows a sample of the template fitting process result, presenting the same body in a different topology, maintaining consistency.

Figure 4.4 – Correlation of the incrementing interval(ΔT) to the average error.

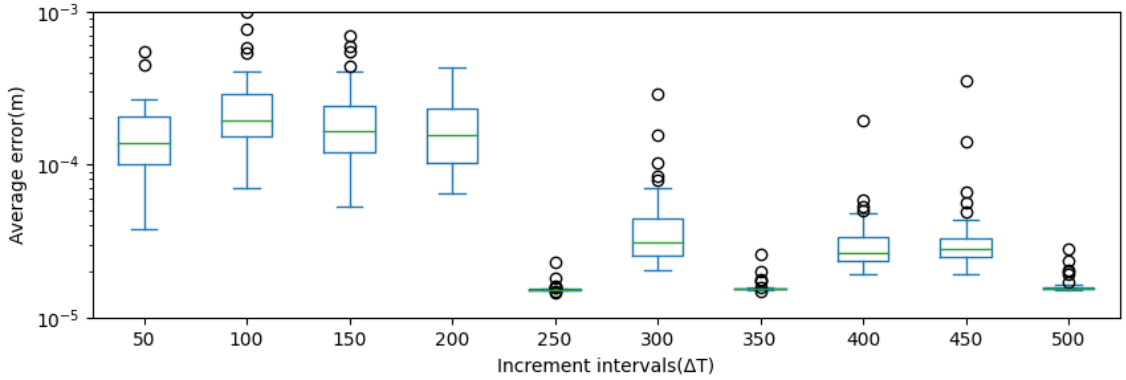

Source: The Author.

4.2.2 Surface Smoothing

This step describes the mesh smoothing process used in our methodology. We wanted to investigate how increasing the number of polygons representing the mesh would affect the quality of measurements. To achieve surface smoothing in the body meshes, we applied Loop Subdivision (LOOP, 1987). Since SMPL models have a consistent topology, and Loop Subdivision maintains its consistency, we could maintain the overall topology of vertices in the body while also smoothing out the surface. Figure 4.9 (b,c) presents a

Figure 4.5 – Correlation of the incrementing interval(ΔT) to the number of interactions.

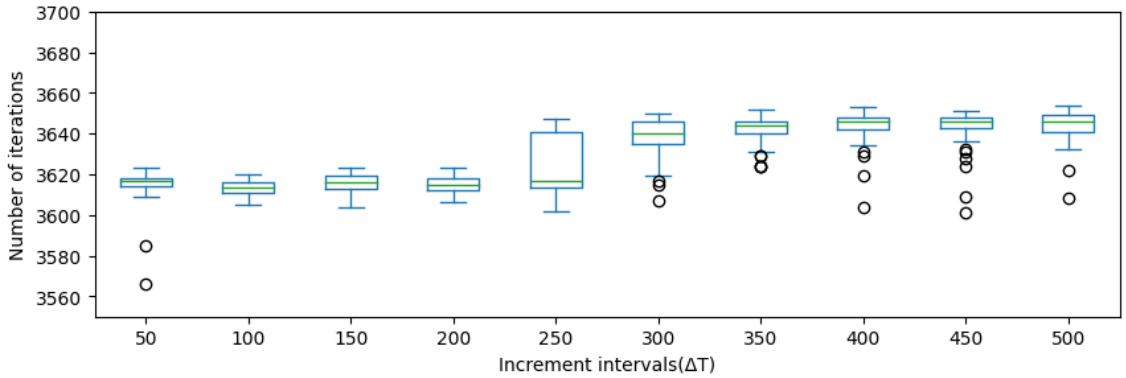

Source: The Author.

Figure 4.6 – Correlation of the incrementing step(ΔPC) to the number of interactions in the interval of increments(ΔT) 200.

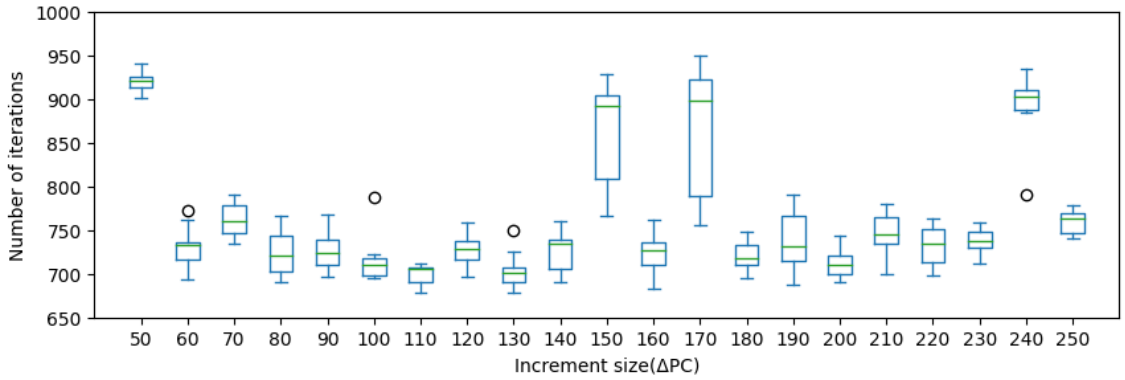

Source: The Author.

sample of this process. We applied a subdivision technique iteratively for each template such that the execution time would not be greater than the time spent in the Template Fitting process. Due to the exponential increase in time when increasing the number of subdivisions, we selected the second subdivision level, generating 220k triangle models. This process reduced the error in computed overall measurements, around 7% for male models and 6.9% for female models.

4.3 Curve Selection

In this step, we want to find the best curve representing a given body measure. Among the many available human body measures, Table 4.4 presents the ones used in this work. Together, they form a subset needed in many applications. The girths were chosen mainly because no specific point landmarks are needed, and girth measurements correlated the most with health issues (HARTZ; RUPLEY; RIMM, 1984; FRENZEL et

Figure 4.7 – Correlation of the incrementing step(ΔPC) to the number of interactions in the interval of increments(ΔT) 250.

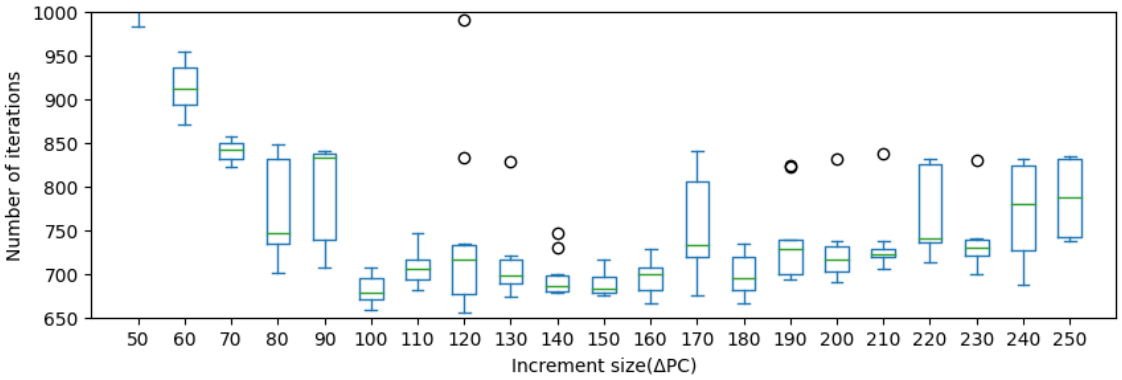

Source: The Author.

Figure 4.8 – Correlation of the incrementing step(ΔPC) to the number of interactions in the interval of increments(ΔT) 300.

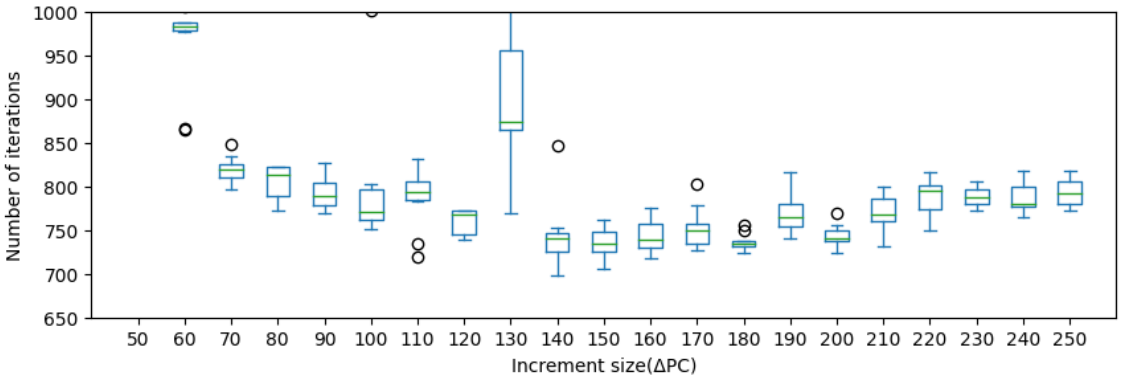

Source: The Author.

al., 2020).

We apply the curve selection procedure in repetition one and validation in repetition two of the MOVE4D subjects. For the 72 bodies, we computed the average male and female bodies. For each average body, we perform horizontal and vertical slicing $1mm$ apart, resulting in around 7500 curves (the exact number varies according to the stature of each body). The slicing is computed as the intersection of planes with the body geometry. We then transfer a subset of these curves according to the measures in Table 4.4 to the 72 bodies, according to their gender, calculate the length of each curve, and compare against our ground truth defined as the equivalent measurements from the MOVE4D station, since it proved the most consistent in Ballester et al. (2022) work. The best curve representing a particular measurement is the one that minimizes the average error among the bodies. We now explain these steps in more detail.

Figure 4.9 – Sample presenting the original model (a), template fitted model (b), and 220k triangles smoothed model (c).

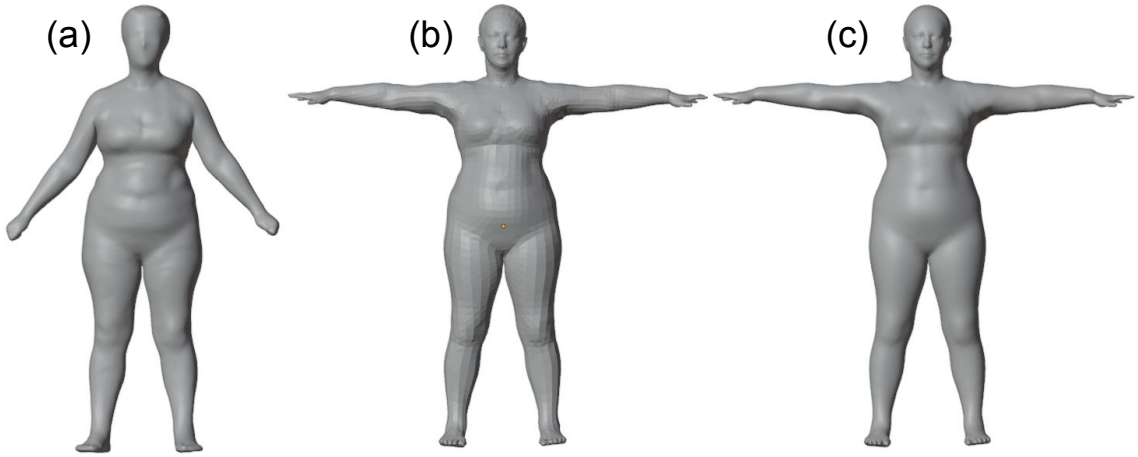

Source: The Author.

Table 4.4 – Used measures, corresponding ISO identifier, and difference in millimeters between our measurements and MOVE4D (BALLESTER et al., 2022) in the curve selection process for the male (M) and female (F) cases.

Measure	**ISO 8559 (2017) Identifier**	**AVG(mm)**		**STD(mm)**	
		M	**F**	**M**	**F**
Bust Girth	5.3.4	11.82	17.48	10.46	12.65
Waist Girth	5.3.10	5.69	10.80	4.00	9.54
Hip Girth	5.3.13	4.52	11.92	3.37	10.88
Thigh Girth	5.3.20	6.90	8.27	5.09	7.42
Upper Arm Girth	5.3.16	3.13	5.42	2.05	3.58
Neck Girth	5.3.2	6.93	4.94	5.74	3.40
Neck To Waist	5.4.5	12.07	7.70	7.31	6.61

4.3.1 Curve-level Planes Slicing

We use a plane intersection technique to cut the body into curve levels, determining the intersection point of each mesh edge with the slicing planes, with each slice only $1mm$ thick. We do this vertically and horizontally, illustrated in Figure 4.10 (a). In the case of the neck, we also search for the best angle from $0°$ to $30°$ to rotate the plane since the neck girth is not an axis-aligned measure. We select the range $(0, 30)$ according to data in ISO (ISO, 2017). Figure 4.11 presents a neck intersection plane, ensuring the correctly sorted curve intersection points. We use barycentric coordinates to represent the intersection points, allowing us to transfer this slice to any other similar mesh and calculate each measure as the sum of Euclidean distances between adjacent vertices in clockwise order.

Figure 4.10 – Body vertical curve slicing illustration (a), Selected curves sample (b), and bounding box filters (c).

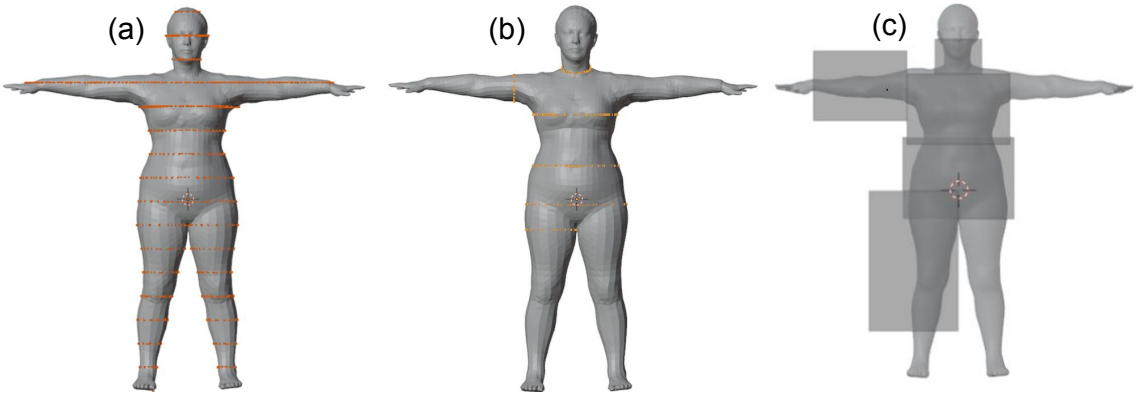

Source: The Author.

Figure 4.11 – Curve-level approach applied on a neck girth. Plane intersection with the mesh at the neck (a), set of computed intersection points unsorted (b), followed by the sorted set (c). The color scale presents the order of vertices.

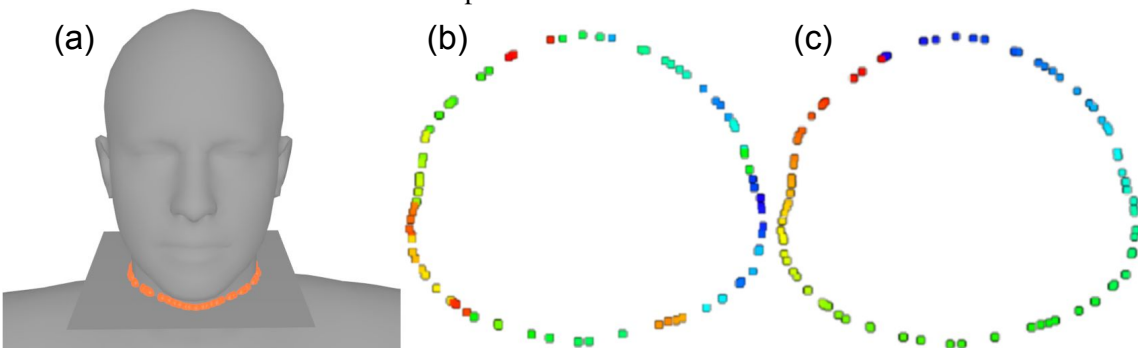

Source: The Author.

4.3.2 Bounding Box Filter

When using infinite planes in our curve-level approach, there are situations where the plane intersection extends beyond the measuring zone, such as the legs and arms. We use bounding boxes to narrow down the plane-body search intersection areas, *i.e.*, reduce the search space. These boxes are defined by the body stature, body width, and heuristics based on Head Unit (HU) ratios used in technical drawing (SZKUTNICKA, 2010) as a reference to calculate size and position. The body width was calculated as the distance from the left to right extremities of the body in the opened-arm pose. The HU is calculated by dividing body stature by eight. Figure 4.10(c) illustrates a 2D projection of the bounding boxes.

All boxes have 1m of size in the z-axis. All distances above the ground, are in relation to the box floor, *i.e.* the face of the box parallel to the xz plane with a small y value. The rest of each bounding box parameter is defined as follows:

- Neck Box is defined as 0.75 HU as height, 1 HU as width, and 6.5 HU above the ground;
- Bust Box is defined as 1.5 HU as height, 2 HU as width, and 5 HU above the ground;
- Torso Box is defined as 1.75 HU as height, 2.25 HU as width, and 3.5 HU above the ground;
- Leg Box is defined as 3 HU as height, $\frac{1}{4}$ body width as width, 1 HU above the ground, this box is displaced in the x-axis from the origin in $\frac{1}{8}$ body width to the right;
- Arm Box is defined as 1.5 HU as height, 2 HU as width, and 5.5 HU above the ground, this box is displaced in the x-axis from the origin in 1.125 HU to the right.

4.3.3 Curve-level Planes Selection

From the set of all possible planes, the optimal one is chosen based on its between-bodies-mean error, whereby we evaluated the error of each curve level for both genders and computed the mean results for each curve. We select the curve with the lowest mean outcome as the best option.

We present the results of the best-selected curve measurements in comparison with the MOVE4D measurements from Ballester et al. (2022) for the male and female cases in Table 4.4. Figure 4.10(b) presents selected curves in a female subject sample.

4.4 Curve Application

Assuming the topology of the 3D mesh template we are using for measuring is consistent, granted by the SMPL model template, i.e., all the bodies have the same number of triangles and the triangles are in the same location, it is possible to transfer the curve levels from the template to the new meshes using the barycentric coordinates representation discussed before. This transfer helps decrease the processing time required for each unique body measure, improving the capacity to transfer curve-level measurements to various bodies in the same template. Figure 4.12 presents an example illustrating this situation.

Figure 4.12 – Random samples of female bodies illustrating the variation in shapes and consistency of curve transference.

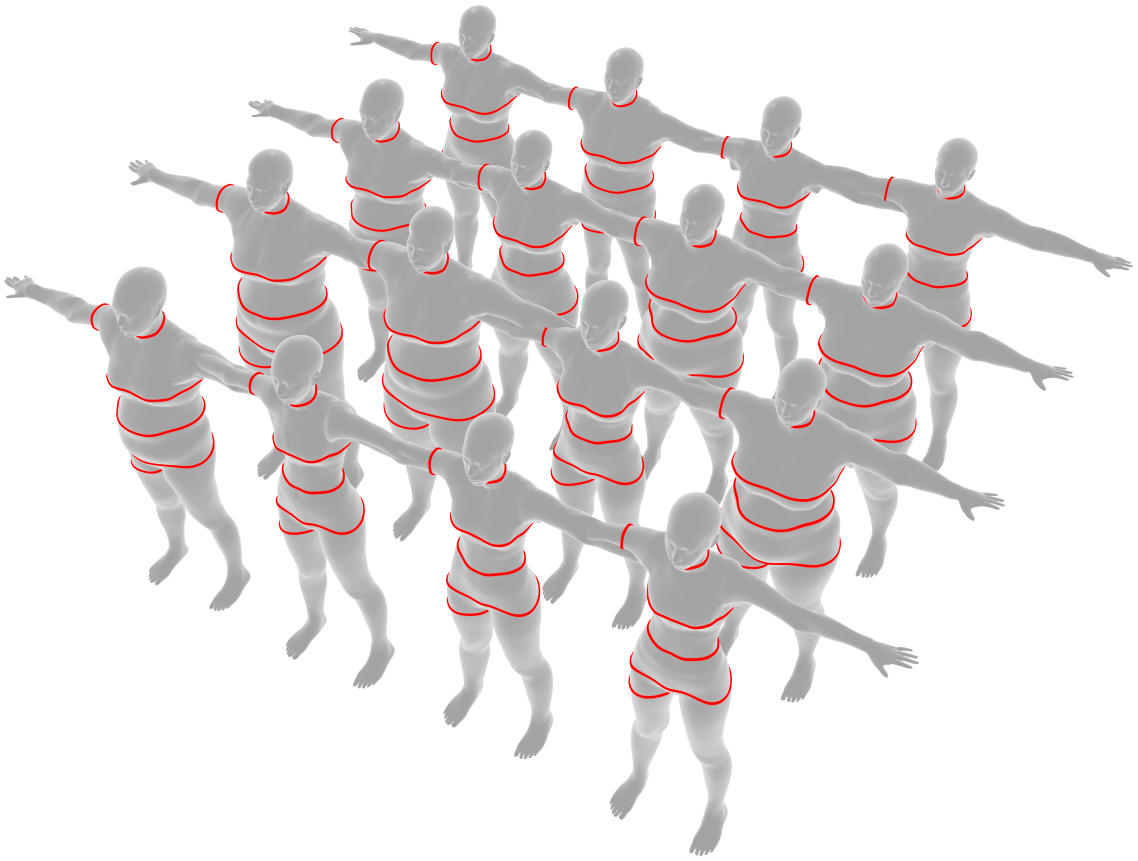

Source: The Author.

5 RESULTS AND DISCUSSIONS

In this chapter, we present the results obtained from the presented approach. Once we complete the established consistent measures, we must check whether they are accurate. We use the appropriate statistical methods proposed by Ballester et al. (2022) to validate the results following established international standards. From phase 1 of their study, we worked with 72 bodies with two repetitions, resulting in 144 measurements set for each measure station in our experiment 1. From phase 2, we worked with 59 bodies, resulting in 118 measurements set for each station in our experiment 2.

We developed our prototype using Python along with PyTorch and Open3D library. We used the Pandas Python library as the base for the statistics computation. The aim is to compare the proposed approach with the two competitors regarding the internal and external agreement (Repeatability and Pairwise compatibility). To assess repeatability, we use the MAD and the SEM indexes and the PSD index to assess pairwise compatibility.

Our validation uses the Ballester et al. (2022) work as a base, although, there are competitors in the literature such as ANET (Nourbakhsh Kaashki; HU; MUNTEANU, 2021). We did not compare with this work because the missing data to reproduce the techniques, and the compatibility analysis, requires the same subset of subjects.

This chapter is divided into *i)* the results obtained in the statistical analysis of our method, *ii)* the standard agreement of our method, and *iii)* the compatibility among other methods in the state-of-the-art.

5.1 Statistical Results

This section discusses the results according to the statistics presented in the previous sections.

5.1.1 Mean Absolute Deviation

Table 5.1 and Table 5.2 present the results obtained for the MAD metric, as well as the agreement with the ANSUR (GORDON et al., 1989) thresholds. We obtained an increment in the state-of-the-art repeatability 7.7% better than MOVE4D and 17.6%

better than SS20 in the average. Furthermore, we increased the compatibility with the ANSUR, compared with the MOVE4D we increased from 6 to 7, comparing with SS20 from 5 to 6, indicating an increment of agreement of 14.2% and 16.6% respectively.

Table 5.1 – MAD for each measure in each selected station (mm). All our measures satisfy ISO error bounds. Compared with the MOVE4D, our average results are 7.7% better. Green highlights the ANSUR MAD agreement.

Measure	Expert	MOVE4D	Our
Bust Girth	12.5347	8.5292	6.8866
Waist Girth	9.1319	6.4874	5.6992
Hip Girth	8.8194	3.0823	3.5551
Thigh Girth	7.8472	2.6278	2.9425
Upper Arm Girth	8.2014	2.7248	2.6521
Neck Girth	5.2431	2.3442	2.6996
Neck to Waist	10.4514	5.1012	4.2303
Average	**8.8899**	**4.4138**	**4.0951**

Table 5.2 – MAD for each measure in each selected station (mm). All our measures satisfy ISO error bounds. Compared with the SS20, our average results are 17.6% better. Green highlights the ANSUR MAD agreement.

Measure	Expert	SS20	Our
Bust Girth	10.1818	7.2961	7.6308
Waist Girth	16.2273	9.7934	7.9020
Hip Girth	13.5000	7.1631	7.1314
Thigh Girth	12.5909	5.8503	6.0895
Upper Arm Girth	5.0000	7.9471	4.5074
Neck Girth	6.5455	5.2261	4.5742
Neck to Waist	11.6364	10.0343	7.4790
Average	**10.8117**	**7.6158**	**6.4735**

5.1.2 Standard Error of Measurements

Table 5.3 and Table 5.4 present the results obtained for the SEM metric, which indicates an increment in the state-of-the-art repeatability 13.9% better than MOVE4D and 0.2% better than SS20, resulting in an average increment of 8.8% according to Standard Error of Measurements.

5.1.3 Pairwise Standard Deviation

Table 5.5 and Table 5.6 present the results obtained for the PSD metric. Considering MOVE4D and SS20 as reference measures, our results compared with Expert are

Table 5.3 – SEM for each measure in each selected station (mm). All measures satisfy ANSUR error bounds. Compared with the MOVE4D, our average results are 13.9% better. Green highlights our results as the best.

Measure	Expert	MOVE4D	Our
Bust Girth	12.2070	7.8704	5.6181
Waist Girth	8.7663	6.4854	5.7769
Hip Girth	7.9468	2.7363	3.0902
Thigh Girth	6.9973	2.5784	2.6602
Upper Arm Girth	12.2280	2.4856	2.5728
Neck Girth	4.8231	2.3343	2.3806
Neck to Waist	9.2412	4.9256	3.7240
Average	**8.8871**	**4.2023**	**3.6890**

Table 5.4 – SEM for each measure in each selected station (mm). All measures satisfy ANSUR error bounds. Compared with the SS20, our average results are 0.2% best. Green highlights our results as the best.

Measure	Expert	SS20	Our
Bust Girth	10.8432	6.3283	6.7248
Waist Girth	17.6614	8.9595	10.2937
Hip Girth	14.9929	6.6426	7.9938
Thigh Girth	11.2816	5.8041	9.0074
Upper Arm Girth	5.1265	7.4835	4.5148
Neck Girth	5.8890	4.8202	4.4899
Neck to Waist	10.2074	11.3672	7.4990
Average	**10.8574**	**7.3436**	**7.2176**

28.5% and 38.8% better respectively.

Table 5.5 – PSD comparisons, including our method vs. Expert and MOVE4D and between MOVE4D and Expert. Green highlights the ISO 20685-1 (ISO, 2018) PSD agreement.

Measure	Our vs Expert	Our vs MOVE4D	MOVE4D vs Expert
Bust Girth	12.04	7.44	10.17
Waist Girth	22.09	20.71	22.39
Hip Girth	23.08	13.25	22.25
Thigh Girth	15.04	11.94	14.79
Upper Arm Girth	16.47	6.01	15.58
Neck Girth	14.58	10.43	11.48
Neck to Waist	19.94	13.73	20.19
Average	**17.60**	**11.93**	**16.69**

5.2 Standards Agreement Discussion

Adopting the described statistics of comparison along with the discussion started by (MARKIEWICZ et al., 2017) and extended by (BALLESTER et al., 2022), our results were compared with the quality specified by ISO 20685-1 (ISO, 2018) and ANSUR

Table 5.6 – PSD comparisons, including our method vs. Expert and SS20 and between SS20 and Expert.

Measure	Our vs Expert	Our vs SS20	SS20 vs Expert
Bust Girth	24.76	16.26	23.69
Waist Girth	32.68	22.16	36.15
Hip Girth	63.85	38.00	54.87
Thigh Girth	34.23	24.56	32.05
Upper Arm Girth	13.53	32.59	33.35
Neck Girth	24.61	17.75	22.15
Neck to Waist	31.42	31.76	33.04
Average	**32.15**	**26.15**	**33.61**

(GORDON et al., 1989), presented in Table 5.7.

According to the mean absolute deviation (MAD), presented in Table 5.1 and Table 5.2, our measures achieve 100% of agreement with the ANSUR MAD threshold in the MOVE4D experiment and 85.7% in the SS20 experiment, compared with 85.7% of agreement with MOVE4D and 71.4% of agreement with SS20, an increment of 14.3% in both cases. Our PSD values are better against MOVE4D than MOVED4D against Expert. According to the presented results, we can see that our compatibility is closer to 3D scanners than Expert. According to the low reliability of Expert, we have a possible justification of MOVE4D, SS20, and our higher PSD values against Expert. In our comparison, we are unique in achieving the ISO 20685-1 (ISO, 2018) in only one measure, the Bust Girth, even though we almost achieved the compatibility in Upper Arm Girth, as we can see in Table 5.5.

Table 5.7 – Measures, ISO, and ANSUR thresholds.

Measure	ANSUR MAD thresholds (mm)	ISO PSD thresholds (mm)
Bust Girth	14	9
Waist Girth	12	9
Hip Girth	12	9
Thigh Girth	6	9
Upper Arm Girth	6	4
Neck Girth	6	4
Neck To Waist	5	5

5.3 State-of-the-Art Compatibility Discussion

Our research findings demonstrate that our results align with the field's current state-of-the-art. Compared with the state-of-the-art metrics MAD and PSD, our result

is 14.2% better in repeatability than the MOVE4D and 16.6% better than the SS20 as illustrated in Figure 5.1, according to compatibility with our results using the scanner as reference measures, our results against Expert is 32.2% for MOVE4D and 18.6% for SS20 better. Our statistics present a close approximation to the scanner results rather than the Expert, as we can see in Figure 5.2, increasing our mistrust about using Expert measures as the ground truth.

Furthermore, our approach offers unique features that set it apart from existing methods, besides an improvement in repeatability and compatibility compared with other state-of-the-art techniques in most cases, such as processing various types of 3D-scanned human bodies. Due to our template-fitting process, our approach is general, *i.e.*, not dependent upon the particular data provided by the scanners used. Also, we do not need scanner measurement data. Additionally, unlike other methods that require manual plane selection, our approach eliminates this process requirement, making it more convenient.

Figure 5.1 – Graph illustrating the MAD results obtained in our experiments, the expert results in the two phases, and the two scanners results and ANSUR threshold (black line).

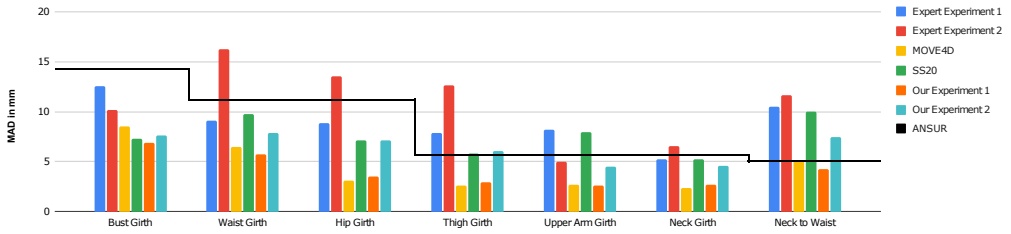

Source: The Author.

Figure 5.2 – Graph illustrating the relative to PSD distance between our compared to other evaluated measurement techniques. Graph layout generated by Force Atlas 2 (JACOMY et al., 2014) using Gephi Software (BASTIAN; HEYMANN; JACOMY, 2009).

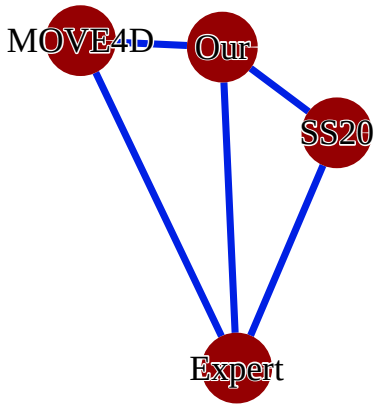

Source: The Author.

6 CONCLUSIONS

We have developed an automated anthropometric measurement system that utilizes curve-level slicing on 3D template-fitted bodies and barycentric coordinates to transfer the measurement definitions to any preprocessed body. Our technique is highly versatile, providing accurate results surpassing the current state-of-the-art by an average of 14.2% and 16.6% in repeatability in comparison of MOVE4D and SS20 and 32.2% and 18.6% in compatibility comparing our result against Expert and against MOVE4D and SS20 scanners. Besides, we improved the number of measures compatible with the thresholds closer than 14.3% compared to both scanners. Compared to other field studies, our approach offers significant advancements. Firstly, it operates entirely automatically, eliminating the need for human intervention. Secondly, it can extract measurements from any body scan. This is made possible by our fitting template process and efficient transfer of measurements across different body shapes.

Our approach, however, has some limitations. Although our method can be applied to all needed body measures, we only tested on girth and one girth-based linear measure, missing landmarks-based linear measures that, although measured on the surface, require knowledge of internal parts of the body. Also, our ability to conduct large-scale comparisons and validations could be improved given more publicly available validated body sets. The proposed approach cannot deal with holes and noisy bodies. The source code of the developed approach was publicly available on the GitHub here.

For future work, we intend to extend the number of considerable measures from the analyzed standards since our 3D models have geometric limitations that make it challenging to work with landmark-based measures. The body's set can be greatly expanded by adding bodies with more issues, for example, holes and noise, with a hole-filling technique to address these issues, like the Iterative Closest Point approach used by some related works.

REFERENCES

ANGUELOV, D. et al. Scape: shape completion and animation of people. In: **ACM SIGGRAPH 2005 Papers**. [S.l.]: ACM New York, NY, USA, 2005. p. 408–416.

BÆRENTZEN, J. A. et al. **Guide to computational geometry processing: foundations, algorithms, and methods**. [S.l.]: Springer Science & Business Media, 2012. 263–264 p.

BALLESTER, A. et al. IEEE SA 3D Body Processing Industry Connections–Comparative Analysis of Anthropometric Methods: Past, Present, and Future. **Comparative Analysis of Anthropometric Methods: Past, Present, and Future**, p. 1–52, 2022.

BALLESTER, A. et al. Data-driven three-dimensional reconstruction of human bodies using a mobile phone app. **International Journal of the Digital Human**, Inderscience Publishers (IEL), v. 1, n. 4, p. 361–388, 2016.

BASTIAN, M.; HEYMANN, S.; JACOMY, M. Gephi: An open source software for exploring and manipulating networks. 2009. Available from Internet: <http://www.aaai.org/ocs/index.php/ICWSM/09/paper/view/154>.

BENABDELKADER, C.; DAVIS, L. Estimation of anthropomeasures from a single calibrated camera. In: IEEE. **7th international conference on automatic face and gesture recognition (FGR06)**. [S.l.], 2006. p. 499–504.

CATMULL, E.; CLARK, J. Recursively generated b-spline surfaces on arbitrary topological meshes. In: **Seminal graphics: pioneering efforts that shaped the field**. [S.l.: s.n.], 1998. p. 183–188.

DAO, N.-L.; DENG, T.; CAI, J. Fast and automatic body circular measurement based on a single kinect. In: IEEE. **Signal and Information Processing Association Annual Summit and Conference (APSIPA), 2014 Asia-Pacific**. [S.l.], 2014. p. 1–4.

De Souza, J. W. et al. Predicting body measures from 2D images using Convolutional Neural Networks. In: IEEE. **Proceedings of the International Joint Conference on Neural Networks**. [S.l.], 2020. p. 1–6. ISBN 9781728169262.

DEVORE, J. L. **Probability and Statistics for Engineering and the Sciences**. [S.l.]: Cengage Learning, 2015. 1–5 p.

DEVORE, J. L. et al. **Modern mathematical statistics with applications**. [S.l.]: Springer, 2012.

DIANAT, I.; MOLENBROEK, J.; CASTELLUCCI, H. I. A review of the methodology and applications of anthropometry in ergonomics and product design. **Ergonomics**, Taylor & Francis, v. 61, n. 12, p. 1696–1720, 2018.

FRENZEL, A. et al. The aging human body shape. **npj Aging and Mechanisms of Disease**, Nature Publishing Group UK London, v. 6, n. 1, p. 5, 2020. ISSN 20563973.

GORDON, C. C. et al. 2012 anthropometric survey of us army personnel: Methods and summary statistics. **Army Natick Soldier Research Development and Engineering Center MA, Tech. Rep**, 2014.

GORDON, C. C. et al. Anthropometric survey of us army personnel: methods and summary statistics 1988. **DTIC Document**, 1989.

HAN, H.; NAM, Y.; CHOI, K. Comparative analysis of 3d body scan measurements and manual measurements of size korea adult females. **International Journal of Industrial Ergonomics**, Elsevier, v. 40, n. 5, p. 530–540, 2010.

HARTZ, A. J.; RUPLEY, D. C.; RIMM, A. A. The association of girth measurements with disease in 32,856 women. **American Journal of Epidemiology**, Oxford University Press, v. 119, n. 1, p. 71–80, 1984.

HU, P. et al. Learning to estimate the body shape under clothing from a single 3-d scan. **IEEE Transactions on Industrial Informatics**, v. 17, n. 6, p. 3793–3802, 2021.

HUGHES-HALLETT, D.; GLEASON, A. M.; MCCALLUM, W. G. **Calculus: Single and multivariable**. [S.l.]: John Wiley & Sons, 2012. 681–684 p.

HUGHES, J. F.; FOLEY, J. D. **Computer graphics: principles and practice**. [S.l.]: Pearson Education, 2014. 172–420 p.

ISO. Size designation of clothes — Part 1: Anthropometric definitions for body measurement. **ISO 8559-1:2017**, p. 80, 2017.

ISO. 3-D Scanning Methodologies for Internationally Compatible Anthropometric Databases. **ISO 20685-1:2018**, 2018.

JACOMY, M. et al. Forceatlas2, a continuous graph layout algorithm for handy network visualization designed for the gephi software. **PloS one**, Public Library of Science San Francisco, USA, v. 9, n. 6, p. e98679, 2014.

JEON, S. et al. Machine learning-based obesity classification considering 3d body scanner measurements. **Scientific Reports**, Nature Publishing Group UK London, v. 13, n. 1, p. 3299, 2023.

JONES, P. R.; RIOUX, M. Three-dimensional surface anthropometry: Applications to the human body. **Optics and Lasers in Engineering**, v. 28, n. 2, p. 89–117, 1997. ISSN 0143-8166. Applications of the Automated Measurement of Human Size and Shape.

KINGMA, D. P.; BA, J. Adam: A method for stochastic optimization. **arXiv preprint arXiv:1412.6980**, 2014.

KOHLSCHÜTTER, T.; HEROUT, P. Automatic human body parts detection in a 2d anthropometric system. In: SPRINGER. **Advances in Visual Computing: 8th International Symposium, ISVC 2012, Rethymnon, Crete, Greece, July 16-18, 2012, Revised Selected Papers, Part II 8**. [S.l.], 2012. p. 536–544.

KOROSTELEVA, M.; LEE, S.-H. Neuraltailor: Reconstructing sewing pattern structures from 3d point clouds of garments. **ACM Transactions on Graphics (TOG)**, ACM New York, NY, USA, v. 41, n. 4, p. 1–16, 2022.

KRZESZOWSKI, T. et al. System for estimation of human anthropometric parameters based on data from kinect v2 depth camera. **Sensors**, v. 23, n. 7, 2023. ISSN 1424-8220. Available from Internet: <https://www.mdpi.com/1424-8220/23/7/3459>.

LEONG, I.-F.; FANG, J.-J.; TSAI, M.-J. Automatic body feature extraction from a marker-less scanned human body. **Computer-Aided Design**, Elsevier, v. 39, n. 7, p. 568–582, 2007.

LIN, Y.-L.; WANG, M.-J. J. Automated body feature extraction from 2d images. **Expert Systems with Applications**, v. 38, n. 3, p. 2585–2591, 2011. ISSN 0957-4174. Available from Internet: <https://www.sciencedirect.com/science/article/pii/S0957417410008444>.

LOOP, C. Smooth subdivision surfaces based on triangles. 1987.

LOPER, M. et al. SMPL: A skinned multi-person linear model. **ACM Transactions on Graphics**, ACM New York, NY, USA, v. 34, n. 6, p. 1–16, 2015. ISSN 15577368.

LOVATO, C. et al. Computer assisted estimation of anthropometric parameters from whole body scanner data. In: SPRINGER. **Modelling the Physiological Human: 3D Physiological Human Workshop, 3DPH 2009, Zermatt, Switzerland, November 29–December 2, 2009. Proceedings**. [S.l.], 2009. p. 71–83.

MARKIEWICZ, Ł. et al. 3D anthropometric algorithms for the estimation of measurements required for specialized garment design. **Expert Systems with Applications**, v. 85, p. 366–385, 2017. ISSN 09574174.

MARKOSKI, B.; MARKOSKI, B. **Basic principles of topography**. [S.l.]: Springer, 2018.

NGUYEN, H. T. et al. Automatic anthropometric system development using machine learning. **BRAIN. Broad Research in Artificial Intelligence and Neuroscience**, v. 7, n. 3, p. 5–15, 2016.

Nourbakhsh Kaashki, N.; HU, P.; MUNTEANU, A. Anet: A Deep Neural Network for Automatic 3D Anthropometric Measurement Extraction. **IEEE Transactions on Multimedia**, IEEE, 2021. ISSN 19410077.

PADILLA, C. J.; FERREYRO, F. A.; ARNOLD, W. D. Anthropometry as a readily accessible health assessment of older adults. **Experimental Gerontology**, Elsevier, v. 153, p. 111464, 2021.

PAQUETTE, S. et al. Automated extraction of anthropometric data from 3d images. In: SAGE PUBLICATIONS SAGE CA: LOS ANGELES, CA. **Proceedings of the Human Factors and Ergonomics Society Annual Meeting**. [S.l.], 2000. v. 44, n. 38, p. 727–730.

PEDRETTI, A. et al. Anthropometric characteristics, physical fitness components and technical skills, a comparison between brazilian and portuguese young soccer players. **Rev. andal. med. deporte**, p. 235–238, 2019.

PETERS, J.; REIF, U. **Subdivision surfaces**. [S.l.]: Springer, 2008. 1–2 p.

PHEASANT, S. Bodyspace: Anthropometry, ergonomics and the design of work. CRC Press, p. 3–8, 2002.

PLEUSS, J. D. et al. A machine learning approach relating 3d body scans to body composition in humans. **European journal of clinical nutrition**, Nature Publishing Group UK London, v. 73, n. 2, p. 200–208, 2019.

ROBINETTE, K. M. et al. **Civilian american and european surface anthropometry resource (caesar), final report. volume 1. summary**. [S.l.], 2002.

RUMBO-RODRíGUEZ, L. et al. Comparison of body scanner and manual anthropometric measurements of body shape: A systematic review. **International Journal of Environmental Research and Public Health**, v. 18, n. 12, 2021. ISSN 1660-4601.

SAMPAIO, L. R. **Avaliação nutricional**. [S.l.]: EDUFBA, 2012. 73–85 p.

SHETTY, K. et al. Boss: Bones, organs and skin shape model. **arXiv preprint arXiv:2303.04923**, 2023.

SZKUTNICKA, B. **Technical drawing for fashion**. [S.l.]: Laurence king publishing, 2010.

TSOLI, A.; LOPER, M.; BLACK, M. J. Model-based anthropometry: Predicting measurements from 3d human scans in multiple poses. In: IEEE. **IEEE winter conference on applications of computer vision**. [S.l.], 2014. p. 83–90.

WEIR, J. P.; VINCENT, W. J. **Statistics in kinesiology**. [S.l.]: Human Kinetics Publishers, 2020.

XIAOHUI, T. et al. Automatic human body feature extraction and personal size measurement. **Journal of Visual Languages and Computing**, Elsevier Ltd, v. 47, n. February, p. 9–18, 2018. ISSN 1045926X. Available from Internet: <https://doi.org/10.1016/j.jvlc.2018.05.002>.

YAN, S.; WIRTA, J.; KÄMÄRÄINEN, J.-K. Silhouette body measurement benchmarks. In: IEEE. **2020 25th International Conference on Pattern Recognition (ICPR)**. [S.l.], 2021. p. 7804–7809.

YANG, G. et al. Geometry processing with neural fields. In: RANZATO, M. et al. (Ed.). **Advances in Neural Information Processing Systems**. Curran Associates, Inc., 2021. v. 34, p. 22483–22497. Available from Internet: <https://proceedings.neurips.cc/paper_files/paper/2021/file/bd686fd640be98efaae0091fa301e613-Paper.pdf>.

YANG, Y. et al. Semantic parametric reshaping of human body models. In: IEEE. **2014 2nd International Conference on 3D Vision**. [S.l.], 2014. v. 2, p. 41–48.

ZAKARIA, N.; GUPTA, D. **Anthropometry, apparel sizing and design**. [S.l.]: Woodhead Publishing, 2019. 3–5 p.

ZHOU, J.; BOONSTRA, J.; KOSINKA, J. Subdivision shading for catmull-clark and loop subdivision surfaces with semi-sharp creases. **Computers**, MDPI, v. 12, n. 4, p. 85, 2023.

ZHOU, Q.-Y.; PARK, J.; KOLTUN, V. Open3d: A modern library for 3d data processing. **arXiv preprint arXiv:1801.09847**, 2018.

ZOU, H.; HASTIE, T. Regularization and variable selection via the elastic net. **Journal of the Royal Statistical Society Series B: Statistical Methodology**, Oxford University Press, v. 67, n. 2, p. 301–320, 2005.

APPENDIX A — RESUMO EXPANDIDO

Processamento e medição do corpo humano 3D

Wesley Ferreira de Ferreira, Marcelo Walter
Instituto de Informática – Universidade Federal do Rio Grande do Sul (UFRGS)

Palavras-chave: Modelagem Geométrica; Medição Antropométrica Automática; Corpos Escaneados

Introdução

Muitas aplicações importantes exigem medições do corpo humano corretas e precisas: compreensão da composição corporal, avaliação de riscos à saúde, design de roupas personalizadas, criação de estações de trabalho ergonômicas e desenvolvimento de programas de condicionamento físico personalizados. Os pesquisadores continuam a explorar novos métodos e tecnologias para melhorar a qualidade das medidas. A tecnologia de digitalização 3D, por exemplo, surgiu como uma ferramenta para medições corporais capturando o volume e a forma do corpo de forma precisa e não invasiva.

Para o desenvolvimento sustentável e comparação de técnicas de medições, a definição de padrões por órgão reguladores, como a ISO, ficou clara, sendo iniciadas na década de 90 e em desenvolvimento até os dias de hoje. Apesar dos esforços para o desenvolvimento desses padrões, atingir o nível de qualidade recomendado ainda é desafiador, requer equipamentos apropriados, treinamento e experiência. Mesmo com esses requisitos, erros ainda ocorrem devido a diversos fatores, como movimentos, roupas e postura.

Nossa principal motivação é expandir as bases comparativas das técnicas de medição corporal digitalizada em 3D e, ao mesmo tempo, aumentar a repetibilidade e a compatibilidade por meio de nossa abordagem, tendo como principal objetivo criar um método que meça corpos humanos de forma rápida, automática e precisa, seguindo padrões internacionais, através de um processo sistemático usando estatísticas no estado-da-arte e comparando também com técnicas do estado-da-arte.

Materiais e Métodos

O trabalho foi dividido em três etapas: *i)* pré-processamento corporal, onde convertemos um conjunto de malhas corporais 3D que queremos medir em um modelo SMPL equivalente; *ii)* seleção de curvas, onde primeiro calculamos um corpo médio como o corpo base do nosso conjunto de corpos, e neste corpo base, encontramos a melhor curva correspondente na superfície do corpo para cada medida desejada; e *iii)* aplicação de curvas, onde

transferimos as curvas do corpo base para todos os demais corpos do conjunto, finalizando as medições.

As malhas corporais em 3D e os dados antropométricos usados para este trabalho, bem como os experimentos realizados foram divididos em dois: o primeiro experimento, usando malhas do digitalizador MOVE4D e medidas antropométricas extraídas por um especialista, consiste em um conjunto de sujeitos de 36 homens e 36 mulheres; o segundo experimento, utilizando malhas do digitalizador SS20 e medidas antropométricas também extraídas por um especialista, consiste em um conjunto de sujeitos de 20 homens e 39 mulheres.

Foi desenvolvido um procedimento computacional que para cada corpo, interativamente otimiza os valores apropriados das Componentes Principais (PCs) usando como critério de erro a distância entre o corpo original e o modelo. Este processo é feito usando o otimizador Adam com taxa de aprendizagem de 0.2 com critério de parada de 0.2mm e em complemento a conversão foi realizado um processo de suavização dos corpos devido a baixa resolução do modelo original e ao pontencial de melhora das medidas.

Na segunda etapa queremos encontrar a melhor curva que representa uma determinada medida corporal. Para isso um processo de segmentação em curvas de nível através de um plano de corte é aplicado, segmentando o corpo vertical e horizontalmente, e em variação de ângulo no caso do pescoço, restringindo as curvas de nível em áreas de interesse através de caixas delimitadoras. Para a seleção das curvas mais adequadas, as mesmas foram transferidas para vários corpos através de posicionamento de coordenadas baricêntricas, onde foram medidas e comparadas com a base de dados MOVED4, onde as curvas selecionadas foram as que na média entre os corpos minimizam as diferenças.

A terceira etapa se atém à transferência das curvas selecionadas na etapa anterior para outros corpos processados da mesma forma através da mesma abordagem de coordenadas baricêntricas, a validação visual das curvas e a medição propriamente dita.

Resultados e Discussões

Uma vez estabelecidas as medições consistentes, é necessário avaliar a acurácia. Foi adotada uma estratégia de validação baseada em duas métricas propostas pelo estado-da-arte em avaliação estatística aplicado a medidas antropométricas: o *Mean Absolute Deviation*, para avaliar a repetibilidade do processo de medição, e o *Pairwise Standard Deviation*, para avaliar a compatibilidade das medidas com as de outras técnicas, bem como foram usados os limiares padronizados internacionalmente de cada uma dessas métricas.

Em relação a avaliação realizada, em relação a repetibilidade foi notado um incre-

mento de 14.2% no primeiro experimento e 16.2% no segundo, em relação a compatibilidade, os experimentos apresentaram um incremento de 32.2% e 18.6% respectivamente. Além disso, na avaliação de compatibilidade, nota-se um incremento de 14.3% na concordância com os limiares internacionais.

Por fim, pode-se notar uma concordância maior entre os métodos de antropometria digitais em comparação com o especialista, bem como uma repetibilidade menor nas medidas dos mesmos, o que indica que embora a antropometria tradicional seja considerada o padrão ouro de avaliação, a antropometria digital apresenta resultados mais coerentes.

Conclusão

Desenvolvemos um sistema automatizado de medição antropométrica que utiliza corte em curva de nível em corpos ajustados em modelos 3D e coordenadas baricêntricas para transferir as definições de medição para qualquer corpo pré-processado. Nossa técnica é versátil, fornecendo resultados precisos superando o estado-da-arte atual em média de 14,2% e 16,6% em repetibilidade em comparação com MOVE 4D e SS 20 e 32,2% e 18,6% em compatibilidade comparando nosso resultado com Expert e contra scanners MOVE4D e SS20. Além disso, melhoramos o número de medidas compatíveis com os limiares próximos a 14,3% em comparação com ambos os scanners. Nossa abordagem oferece avanços significativos: em primeiro lugar, funciona de forma automatizada, eliminando a necessidade de intervenção humana; em segundo lugar, pode extrair medidas de qualquer digitalização corporal. Isto é possível graças ao nosso processo de ajuste de modelo e transferência eficiente de medições.

Nossa abordagem tem algumas limitações, testamos apenas as medidas de circunferências e uma medida linear baseada nas circunferências, faltando medidas lineares baseadas em pontos de referência. Além disso, nossas validações poderiam ser aprimoradas com mais conjuntos de corpos disponíveis publicamente. Para trabalhos futuros, pretendemos ampliar o número de medidas, uma vez que nossos modelos 3D possuem limitações geométricas que tornam desafiador trabalhar com medidas baseadas em pontos de referência. O conjunto de corpos pode ser bastante expandido adicionando corpos com mais problemas, por exemplo, buracos e ruído, com uma técnica de preenchimento de buracos para resolver esses problemas, como a abordagem *Iterative Closest Point* usada por alguns trabalhos relacionados.